Title

Meta-Analysis of Nanoparticle Distribution in Tumors and Major Organs in Tumor-Bearing Mice.

Journal

ACS Nano, 17(20)

Authors

Chen, Qiran

Yuan, Long

Chou, Wei-Chun

et al.

Publication Date

2023-10-24

DOI

10.1021/acsnano.3c04037

ACS NANO

www.acsnano.org

ARTICLE

Meta-Analysis of Nanoparticle Distribution in Tumors and Major Organs in Tumor-Bearing Mice

Qiran Chen,[⊕] Long Yuan,[⊕] Wei-Chun Chou, Yi-Hsien Cheng, Chunla He, Nancy A. Monteiro-Riviere, Jim E. Riviere, and Zhoumeng Lin*

Cite This: *ACS Nano* 2023, 17, 19810−19831

Read Online

ACCESS | Metrics & More | Article Recommendations | Supporting Information

ABSTRACT: **Low tumor delivery efficiency is a critical barrier in cancer nanomedicine. This study reports an updated version of "Nano-Tumor Database", which increases the number of time-dependent concentration data sets for different nanoparticles (NPs) in tumors from the previous version of 376 data sets with 1732 data points from 200 studies to the current version of 534 data sets with 2345 data points from 297 studies published from 2005 to 2021. Additionally, the current database includes 1972 data sets for five major organs (i.e., liver, spleen, lung, heart, and kidney) with a total of 8461 concentration data points. Tumor delivery and organ distribution are calculated using three pharmacokinetic parameters, including delivery efficiency, maximum concentration, and distribution coefficient. The median tumor delivery efficiency is 0.67% injected dose (ID), which is low but is consistent with previous studies. Employing the best regression model for tumor delivery efficiency, we generate hypothetical scenarios with different combinations of NP factors that may lead to a higher delivery efficiency of >3%ID, which requires further experimentation to confirm. In healthy organs, the highest NP accumulation is in the liver (10.69%ID/g), followed by the spleen 6.93%ID/g and the kidney 3.22%ID/g. Our perspective on how to facilitate NP design and clinical translation is presented. This study reports a substantially expanded "Nano-Tumor Database" and several statistical models that may help nanomedicine design in the future.**

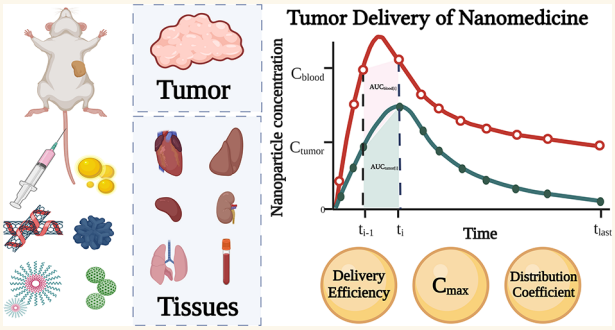

KEYWORDS: *Nanoparticle, Tumor delivery, Tissue distribution, Cancer, Nanomedicine*

A number of studies have shown that nanoparticles (NPs) or NP-based drug formulations are effective as diagnostic agents to detect tumors or as therapeutic agents to treat cancer in preclinical models, including mice and rats.[1] Compared to conventional drug delivery systems, NP-based systems have several advantages, potentially including high stability with a longer half-life, high carrier capacity, precise delivery to the targeted tissue to reduce toxic side effects, and high drug bioavailability.[2,3] However, in the last 20 years, only a small number of NP-based drug formulations have been successfully translated for clinical use in humans.[4,5] The reasons for this low clinical translation rate are, in part, due to very low delivery efficiency (DE) of NPs to the tumor site and insufficient understanding of interactions between NPs and cells.[6,7]

To improve the targeting DE of NPs to tumors and reduce their adverse effects in the rest of the body, the main approach is to optimize the targeting strategy through active targeting to a tumor site or to increase the enhanced permeability and retention (EPR) effect and improve NP's physicochemical properties, such as the core material, surface charge, size, and shape.[8] In addition, numerous studies have investigated the impacts of NP design on tumor DE. Several meta-analyses were conducted to summarize tumor DE of different types of NPs and to determine the impacts of physicochemical properties on NP delivery to tumors. For example, Wilhelm et al. (2016)[5] analyzed the literature data on NP distribution to tumors published from 2005 to 2015 using a traditional noncompartmental pharmacokinetic (PK) approach and reported a median tumor DE of 0.7% of the injected dose

Received: May 5, 2023
Accepted: August 24, 2023
Published: October 9, 2023

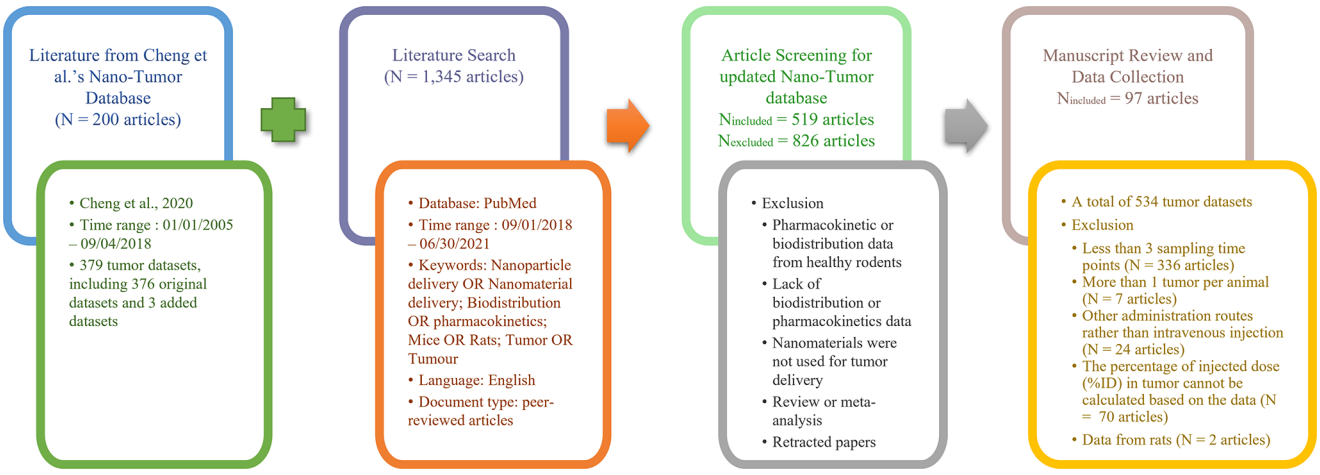

Figure 1. Flowchart and inclusion/exclusion criteria for the literature search and data collection. Built upon the Cheng et al. "Nano-Tumor Database" that contains 376 data sets on nanoparticle tumor delivery from 200 studies published from 01/01/2015 to 09/04/2018,[9] we included an additional 97 studies with 158 data sets from 09/01/2018 to 06/30/2021. As a result, the total number of data sets in the updated "Nano-Tumor Database" is 534 with a total of 2345 data points for tumors. Note: among 158 collected data sets, 155 data sets were from the 97 newer studies and the remaining 3 data sets from three earlier studies that were not collected in the original version of "Nano-Tumor Database". For healthy major organs, there are 1972 data sets: 340 for heart, 456 for liver, 367 for lung, 413 for spleen, and 396 for kidney with a total of 8461 concentration data points. Please refer to the Supporting Information "Nano-Tumor Database" Excel file for details about the data.

(ID) following intravenous (IV) administration. Based on the Wilhelm et al. study, Cheng et al. (2020)[9] collected additional NP tumor DE data from 2005 to 2018 (termed as "Nano-Tumor Database" thereafter) and constructed a physiologically based pharmacokinetic (PBPK) model of NPs in tumor-bearing mice. Using the PBPK model, Cheng et al. were able to predict NP DE in tumors at 24 and 168 h after IV administration, and at the last sampling time point, as well as the maximum DE.[9] However, this study found that NP tumor DE did not improve from 2015 to 2018 because the median DE remained at 0.76% injected dose (ID). Low NP tumor DE was also associated with low distribution and permeability coefficients at the tumor site.[9]

The trend of NPs' tumor DE did not increase over time, which indicates little improvement in tumor DE of NPs over the last 20 years and represents a critical barrier in the field of nanomedicine.[5,9−11] One of the potential reasons for this stagnation is the inadequate analysis of some crucial factors in computational analysis and the lack of taking the impacts of these factors into consideration for NP design scenarios. Therefore, it is essential to evaluate and interpret the tumor delivery of NPs from alternative perspectives. Price et al. (2020)[10] reanalyzed the NP tumor delivery data from the Wilhelm et al. study[5] with other parameters (e.g., the maximum observed concentration [C_{max}] and area under the curve ratio [AUC_{tumor}/AUC_{blood} ratio]).[10] The authors found that the median tumor/blood AUC ratio was substantially different (i.e., ∼100-fold) from the %ID result from the Wilhelm et al. study.[5] Later, based on the data from the Cheng et al. study,[9] another research group (Fan et al., 2021)[11] reported that it was important to consider the physiological parameters including blood flow and NP-specific parameters such as cellular uptake in the analysis of NP tumor delivery data. In addition, since NP tumor DE is generally low (i.e., <1%ID), a large proportion of the ID is distributed to healthy organs and tissues. Thus, changes in the distribution to healthy organs and tissues could also substantially affect tumor DE. Therefore, it is important to analyze whole-body NP distribution, not only tumors but also blood and healthy organs, in order to fully understand the key determinants of NP tumor delivery.

To address the aforementioned challenges, the objectives of the present study were: (1) to perform a systemic literature search to curate and collect recently published NP tissue distribution and tumor delivery data to expand the "Nano-Tumor Database"; (2) to evaluate the NP delivery to tumors and healthy organs/tissues using different PK parameters; and (3) to identify key physiological and physicochemical determinants of NP tissue distribution and tumor delivery. The updated "Nano-Tumor Database" is provided in the Supporting Information of this article. Compared to our earlier version of the "Nano-Tumor Database",[9] the current study expanded the number of tumor time-dependent concentration data sets from 376 to 534 and added 1972 recently published data sets for major organs (i.e., liver, spleen, lungs, kidneys, and heart) with a total of more than 10,000 concentration data points for both tumors and major organs. The tumor delivery was calculated with both classical AUC-based DE and two other PK parameters (C_{max} and tumor/blood distribution coefficient) in two different units (%ID and %ID/g tissue). Moreover, the analysis of organ distribution implies competitive roles of major reticuloendothelial system (RES) organs in tumor delivery of NPs. The best multivariate regression models were used to generate hypothetical scenarios with a combination of parameters that might result in a higher tumor DE of >3 or even >5%ID, which provides a basis to design more effective nanomedicines in the future.

RESULTS AND DISCUSSION

Overview of the Methods. Briefly, this study included relevant studies published between 1/1/2005 and 6/30/2021 (Figure 1). The raw tumor concentration data from 200 articles published between 2005 and 2018 were obtained in an earlier study by Cheng et al. (2020).[9] Based on the same inclusion and exclusion criteria, a total of 158 recently published tumor data sets, mainly from 97 articles published

https://doi.org/10.1021/acsnano.3c04037
ACS Nano 2023, 17, 19810−19831

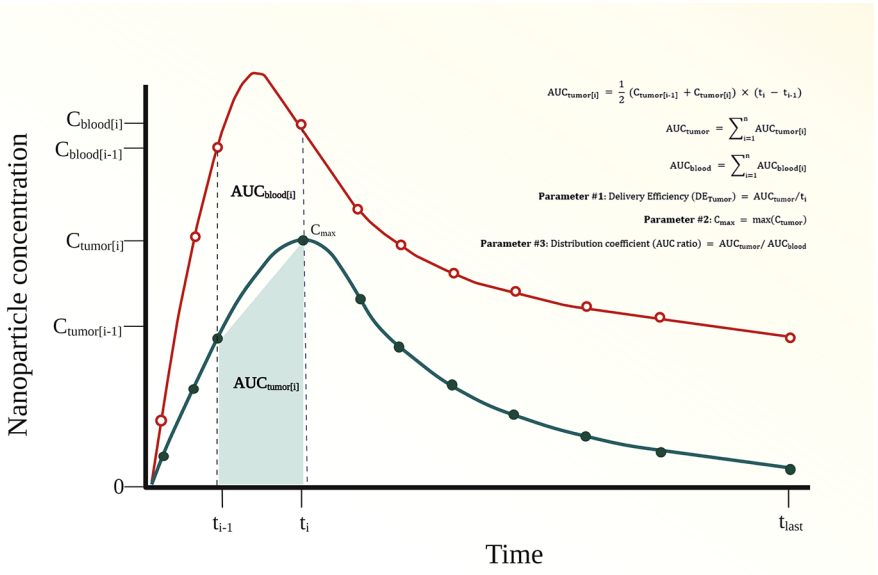

Figure 2. Schematic of PK parameter (delivery efficiency, C_{max}, and distribution coefficient) calculation. The concentration vs time profile in tumor is represented by the solid green dots and green line. The concentration vs time profile in blood is represented by open red circles and red line. The linear trapezoidal method was used to calculate the area-under-the-curve (AUC) for both tumor and blood. The distribution coefficient of tumor is calculated as AUC_{tumor}/AUC_{blood} (This figure was created with BioRender.com).

between 2018 and 2021, was also extracted for analysis in this study.[12−108] Compared to the Cheng et al. study[9] that only collected concentration data in tumor tissues, the present study also extracted the concentration data in the blood and five major organs (heart, liver, spleen, lung, and kidney) from all relevant studies (i.e., a total of 297 articles published between 2005 and 2021) in order to have a more comprehensive understanding of the tissue distribution of NPs in tumor-bearing mice. For each data set, the relevant parameters of the physicochemical properties of the NPs, including the composition, organic/inorganic materials, targeting strategy, zeta potential measured at pH 7.4, surface chemistry, hydrodynamic diameter, core diameter measured via transmission electron microscopy (TEM), polydispersity index (PDI), and shape as well as the experimental methods, including tumor model, cancer type, tumor cell type, tumor size, tumor weight, experimental animal, sex, body weight, strain, administration position, administration dose, and raw NP concentration data in the tumor, blood, and tissues were collected.

To compare data from different articles having different experimental designs and data expressed using different units, the raw concentration data from all studies were collected and converted to the units of "percentage of the injected dose" (%ID) and "%ID per gram of tissue" (%ID/g) (detailed methods are provided in Section 1 of the Supporting Information). Tumor delivery and organ distribution of NPs were calculated using three PK parameters: (1) DE in the unit of %ID or %ID/g tissue calculated based on AUC (the AUC from t-zero to t-last), (2) the maximum observed concentration (C_{max}) in the unit of %ID or %ID/g tissue, and (3) distribution coefficient, which refers to the ratio of tumor and blood AUC (AUC_{tumor}/AUC_{blood}).[10] The details of the calculation are described in the Materials and Methods section and illustrated in Figure 2.

The impacts of physiological and physicochemical properties on the calculated PK parameters were assessed by univariate and multivariate analyses on tumors. The univariate analyses were conducted using one-way analysis of variance (ANOVA) (or the Kruskal−Wallis test as appropriate), while the multivariate analyses were completed using multivariable linear regression. The effects of the physicochemical parameters on the distribution of NPs in major healthy organs were assessed by using a multivariate analysis of variance (MANOVA).

Tumor Delivery of Different Subgroups by the Physicochemical Parameters. The tumor delivery was summarized based on different physicochemical properties and experimental designs of the studies analyzed (Figures 3, 4, and S1−S4; Tables 1 and S1). The number of data sets that involved each of the physicochemical properties was also provided in these tables (designated as the "Count" column). The number of data sets involving passive targeting strategy was much higher than that using active targeting strategy (340 vs 194) (Table 1). The number of data sets on organic NPs was much larger than those of inorganic and hybrid NPs (358 vs 160 vs 16). Among all organic NPs, most of the data sets were on polymeric NPs (59%). In terms of shape, most of the data sets used spherical NPs (84%). Regarding the size, most data sets were in the range from 10−200 nm (72%). In terms of surface charge, the number of data sets using positive-charge NPs was much less than negative or neutral NPs (38 vs 211 vs 212). In terms of tumor models, most studies used allograft or xenograft heterotopic tumor models (77%). For the cancer type, breast cancer was the most often studied among all cancer types (34%).

The tumor DE in different subgroups ranged from 0.29%ID (liposome NPs) to 7.41%ID (dendrimer NPs) with an overall median of 0.67%ID (Figure 3F, Table 1). Compared to the studies published between 2005 and 2018, the collected NP data published from 2018 to 2021 had no increase in the median DE_{tumor} (0.74% vs 0.52%ID, $P = 0.086$). Using the unit of %ID/g, the subgroup DEs were between 0.81%ID/g (NPs in gliomas) and 11.45%ID/g (dendrimer NPs) with a median of 3.45%ID/g (Figure S1, Table 1). The median DE_{tumor} between 2005 and 2018 was 3.41%ID/g, and the corresponding value was 3.61%ID/g for the data between 2018 and 2021.

https://doi.org/10.1021/acsnano.3c04037
ACS Nano 2023, 17, 19810−19831

Table 1. Summary of Tumor Delivery for Different Types of Nanoparticles Using Delivery Efficiency and Maximum Concentration[a]

Category	DE (%ID)	DE (%ID/g)	C_{max} (ID%)	C_{max} (ID%/g)	Count
All data sets	0.67 (2.12)	3.45 (10.28)	1.01 (3.11)	4.96 (15.45)	534
Year					
2005−2009	1.03 (2.00)	4.87 (9.79)	1.77 (3.09)	6.07 (15.62)	52
2010−2015	0.62 (2.11)	3.23 (10.10)	0.92 (3.12)	4.76 (14.59)	261
2016−2021	0.59 (2.15)	3.47 (10.62)	0.94 (3.10)	5.08 (16.43)	221
Targeting Strategy					
Active	0.79 (2.97)	4.12 (14.19)	1.08 (4.22)	5.52 (20.65)	194
Passive	0.61 (1.63)	3.11 (8.05)	0.98 (2.47)	4.65 (12.47)	340
Nanomaterial Type					
Hybrid	1.51 (4.23)	6.59 (17.16)	1.84 (5.59)	8.66 (22.13)	16
Inorganic	0.84 (2.80)	3.85 (10.97)	1.26 (4.06)	5.19 (16.20)	160
Organic	0.54 (1.71)	3.24 (9.67)	0.85 (2.57)	4.80 (14.81)	358
Inorganic Nanomaterial					
Gold	1.17 (3.21)	3.07 (5.79)	1.97 (4.87)	4.41 (8.29)	70
Iron Oxide	0.70 (3.17)	4.11 (31.90)	1.03 (4.91)	4.56 (50.83)	11
Silica	0.65 (2.39)	4.12 (11.25)	0.75 (3.16)	4.89 (15.99)	30
Others	0.65 (2.39)	4.71 (13.50)	1.06 (3.27)	6.49 (19.86)	49
Organic Nanomaterial					
Dendrimer	7.41 (8.48)	11.45 (49.63)	9.32 (11.59)	14.22 (64.33)	14
Hydrogel	0.34 (0.48)	2.76 (3.46)	0.51 (0.86)	4.39 (6.00)	20
Liposome	0.29 (1.57)	1.88 (6.60)	0.44 (2.08)	2.91 (9.01)	48
Polymeric	0.62 (1.37)	3.31 (7.63)	0.92 (2.15)	4.97 (12.07)	211
Others	0.68 (1.88)	3.41 (11.82)	0.77 (2.88)	4.51 (19.94)	65
Shape					
Plate	0.47 (0.93)	3.89 (5.54)	0.70 (1.35)	4.62 (7.95)	21
Rod	1.13 (2.76)	3.61 (15.19)	1.50 (3.89)	6.10 (19.94)	41
Spherical	0.69 (2.17)	3.47 (10.34)	1.02 (3.20)	4.97 (15.80)	450
Others	0.46 (1.00)	2.69 (4.45)	0.72 (1.51)	3.82 (7.01)	22
Hydrodynamic Diameter					
<10 nm	1.22 (2.46)	2.85 (15.43)	1.96 (3.77)	4.16 (20.48)	34
10−100 nm	0.78 (1.98)	3.66 (8.67)	1.14 (2.88)	5.47 (12.67)	180
100−200 nm	0.55 (2.10)	3.54 (10.23)	0.81 (3.22)	4.87 (16.79)	204
>200 nm	0.70 (2.28)	3.06 (13.35)	1.15 (3.22)	5.03 (19.08)	75
Surface Charge					
Negative (<−10 mV)	0.47 (1.75)	2.34 (8.56)	0.73 (2.65)	3.57 (13.71)	211
Neutral (−10 to 10 mV)	0.79 (2.21)	4.00 (9.91)	1.22 (3.26)	5.96 (14.74)	212
Positive (>10 mV)	1.08 (4.23)	2.59 (15.24)	1.57 (5.90)	3.02 (21.17)	38
Tumor Model					
Allograft Heterotopic	0.55 (1.43)	3.27 (6.66)	0.77 (2.13)	4.73 (10.07)	158
Allograft Orthotopic	0.89 (2.20)	2.90 (10.66)	1.24 (3.17)	4.59 (15.70)	64
Xenograft Heterotopic	0.70 (2.20)	3.61 (12.66)	1.02 (3.16)	5.12 (18.97)	252
Xenograft Orthotopic	0.91 (3.49)	2.85 (9.45)	1.45 (5.40)	4.58 (14.58)	60
Cancer Type					
Brain	0.72 (1.22)	3.64 (6.62)	0.91 (1.76)	4.89 (8.42)	27
Breast	0.82 (1.76)	3.49 (10.64)	1.17 (2.49)	4.96 (15.20)	180
Cervix	1.00 (2.30)	6.18 (12.48)	1.54 (3.07)	7.93 (16.11)	37
Colon	0.54 (1.58)	3.10 (6.03)	0.97 (2.47)	6.10 (9.66)	39
Glioma	0.04 (0.86)	0.81 (6.97)	0.07 (1.12)	1.38 (9.05)	11
Liver	0.43 (1.82)	3.41 (9.31)	0.63 (2.70)	4.77 (14.83)	83
Lung	0.36 (3.14)	1.91 (23.63)	0.74 (5.66)	3.43 (45.82)	29
Ovary	0.39 (1.34)	1.08 (1.24)	0.81 (2.98)	2.32 (2.29)	18
Pancreas	0.54 (0.91)	4.22 (6.56)	0.73 (1.46)	6.10 (10.02)	12
Prostate	0.62 (1.24)	2.34 (6.46)	0.98 (1.74)	3.26 (9.08)	17
Sarcoma	1.96 (4.59)	7.52 (27.76)	2.60 (5.95)	9.96 (36.94)	19
Skin	1.23 (4.32)	2.90 (7.08)	2.08 (6.29)	3.76 (10.96)	44
Others	1.31 (2.67)	3.48 (6.43)	2.05 (3.54)	4.86 (8.55)	18

[a]Note: The values of delivery efficiencies are presented as median (mean). Abbreviations: DE, delivery efficiency; C_{max}, maximum concentration.

https://doi.org/10.1021/acsnano.3c04037
ACS Nano 2023, 17, 19810−19831

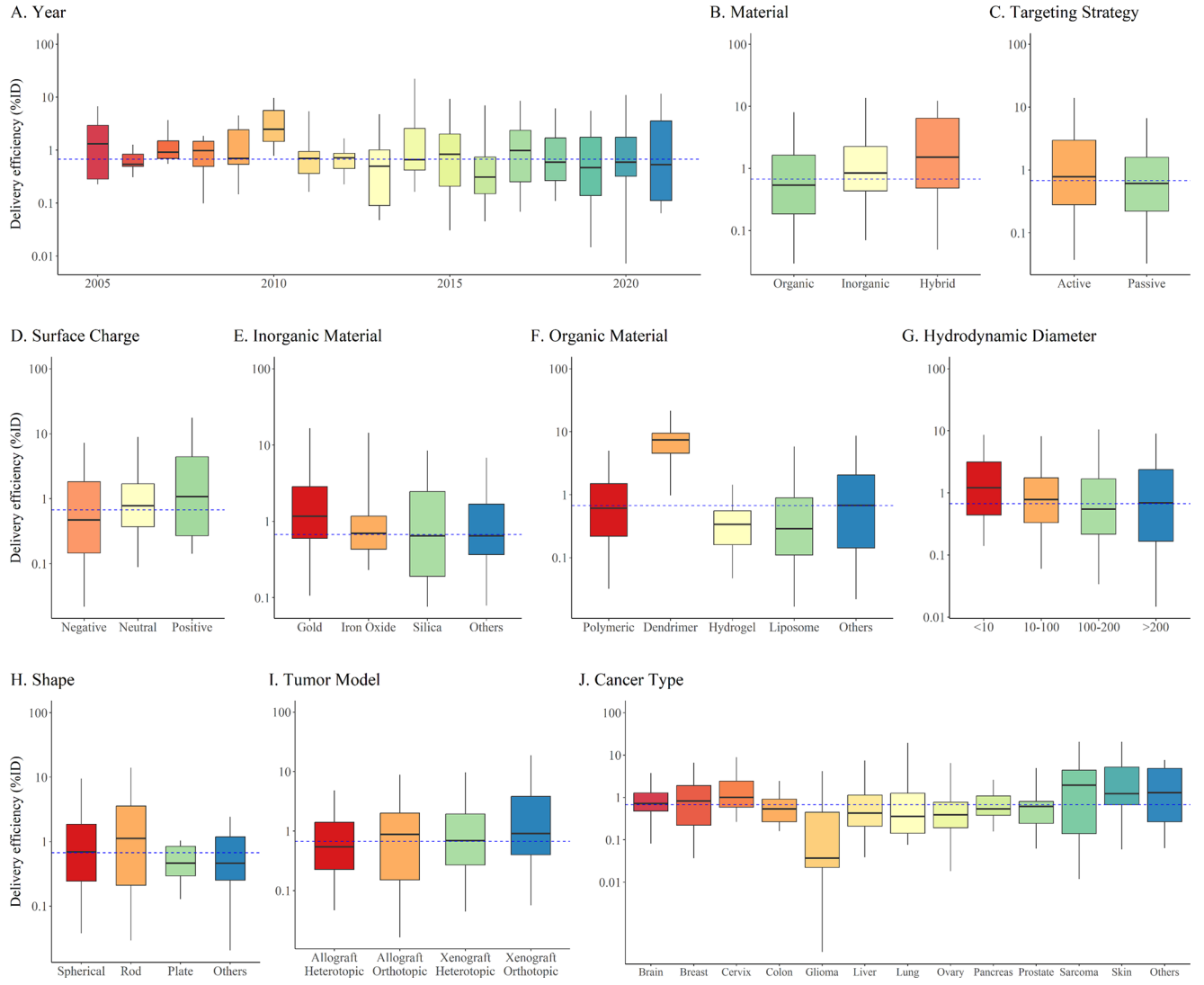

Figure 3. Box-and-whisker plots of the tumor DE data by (A) year, (B) material type, (C) targeting strategy, (D) surface charge, (E) inorganic material, (F) organic material, (G) hydrodynamic diameter, (H) shape, (I) tumor model, and (J) cancer type calculated using the classical AUC method with the unit of injected dose percentage (%ID).[5] The boxes represent the 25th to 75th percentile, and the black lines are the median values. The blue dash lines indicate the overall median of the tumor delivery efficiency derived from all 534 data sets.

There were no significant differences between the earlier data and the more recent data (P = 0.96).

The highest median of subgroup C_{max} was 9.32%ID for dendrimer NPs (Figure S2F, Table 1), while the lowest value was 0.07%ID for the NPs in gliomas (Figure S2J, Table 1), and the overall median C_{max} was 1.01%ID. Compared to the median C_{max} of 1.08%ID based on data between 2005 and 2018, the corresponding value of 0.85%ID for the newer data between 2018 and 2021 was not statistically different (P = 0.15). By taking the tumor weight into account, the maximum and minimum median C_{max} values were 14.22%ID/g for dendrimers and 1.38%ID/g for gliomas, and the overall median C_{max} was 4.95%ID/g. Compared to the result from the earlier version of the "Nano-Tumor Database", the tumor C_{max} did not show a significant increase for the newer data between 2018 and 2021 based on the median values (4.82% vs 5.16% ID/g, P = 0.701).

Additionally, we used the parameters of the tumor/blood distribution coefficient to evaluate the tumor delivery of NP. Within 534 tumor data sets, there were 343 data sets with available blood data. The range for subgroup medians of the % ID-based tumor distribution coefficient data was between 0.04 (NPs in gliomas) and 1.83 (i.e., 1.83-fold in tumor compared to blood for positive-charged NPs) with an overall median of 0.21 (Figure 4, Table S1). The subgroup medians of the tumor distribution coefficient (based on %ID/g) were between 0.20 (NPs in prostate cancer) and 3.44 (positive-charged NPs) with an overall median of 1.03 (Figure S4, Table S1).

In summary, the medians of PK Parameter #1, NP DE, using AUC-based method (0.67%ID and 3.45%ID/g) were comparable to previous meta-analyses.[5,9] Wilhelm et al. (2016)[5] summarized the studies between 2005 and 2015 and calculated the median NP delivery efficiency of 0.7%ID. Cheng et al. (2020)[9] also derived a median NP delivery efficiency in tumor of 0.76%ID at the last sampling time point using the PBPK method. According to these earlier results, it appears there was little improvement in the tumor delivery efficiency of NPs from more recent studies, which is a persistent critical barrier in the field for over the past 15 years. This raises the need to take into account the impact of other factors, such as NP distribution in

https://doi.org/10.1021/acsnano.3c04037
ACS Nano 2023, 17, 19810−19831

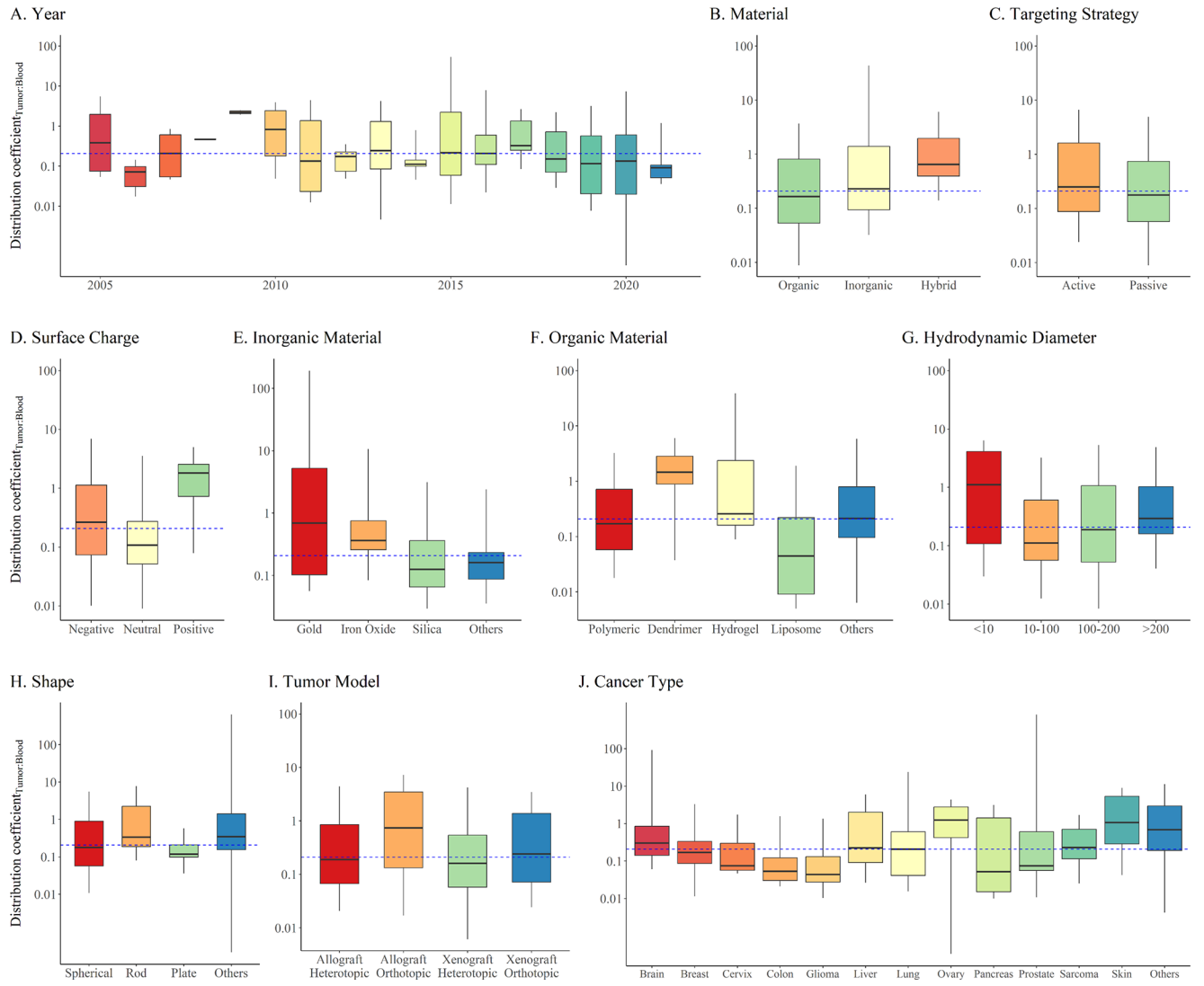

Figure 4. Box-and-whisker plots of the tumor/blood distribution coefficient (PK Parameter #3) data by (A) year, (B) material type, (C) targeting strategy, (D) surface charge, (E) inorganic material, (F) organic material, (G) hydrodynamic diameter, (H) shape, (I) tumor model, and (J) cancer type based on the concentration data in the unit of injected dose percentage (%ID).[10] The boxes represent the 25th to 75th percentile, and the black lines are the median values. The blue dash lines indicate the overall median of the distribution coefficient of 0.21 derived from the 343 data sets that reported the blood data in the original articles.

the blood. Therefore, we applied multiple PK parameters to evaluate the tumor delivery (i.e., DE, C_{max}, and tumor/blood distribution coefficient) and performed regression analyses of tumor delivery by considering the effects of various physicochemical properties and study design factors, as described below.

THE IMPACTS OF INDIVIDUAL PHYSICOCHEMICAL PROPERTIES

Several physicochemical properties have been shown to affect the delivery of NP to the target site, such as particle size, shape, and surface chemistry. These properties may determine the NP tumor entry rate, residence time, penetration depth, and the sequestering proportion by the reticuloendothelial system (RES).[109] Therefore, we collected multiple physicochemical properties of NPs from the enrolled studies and investigated their contributions to NP tumor delivery quantitatively. Before performing the univariate analysis, Shapiro-Wilk normality tests were initially performed, of which results suggested that log-transformed PK parameters were (or more likely to be) normally distributed. Therefore, the log-transformed PK parameters were employed for the following analyses. To evaluate the impacts of single physiochemical properties on the tumor delivery, one-way ANOVA/Kruskal–Wallis test and simple linear regression were conducted for categorical and continuous variables, respectively. The Bartlett's test was used to examine the assumption of equal variance for the one-way ANOVA test. For the data sets that cannot be assumed for equal variance, a Kruskal–Wallis test was performed, which was considered the nonparametric equivalent to a one-way ANOVA.[110] The results showed that the tumor deliveries of NPs were significantly different due to certain physicochemical properties (Tables S2–S4), as described in detail below. Overall, the critical factors that affected tumor delivery of NPs are the core material, surface charge, and cancer type.

To be more specific, the variables that significantly impacted the tumor DE (PK Parameter #1) included NP type, core material, targeting strategy, cancer type, log-transformed

https://doi.org/10.1021/acsnano.3c04037
ACS Nano 2023, 17, 19810–19831

hydrodynamic size [log(HD)], surface charge, and zeta potential (Table S2). In terms of NP type, the tumor DE in organic nanomaterials (ONMs) was much lower than that in inorganic nanomaterials (INMs) (Median: 0.54% vs 0.84%ID; $P = 0.001$) and hybrid NPs (Median: 0.54% vs 1.51%ID; $P = 0.042$), but the difference between INMs and hybrid NPs was insignificant (Median: 0.84% vs 1.51%ID; $P = 0.360$; Table 1 and Table S3). The pairwise comparisons of core material suggested that there were no differences in tumor DE for different types of INMs, while the tumor DE for dendrimer NPs (Median: 7.41%ID) was much higher than that of the group of other ONMs (Medians: 0.29%−0.68%ID). The DE was ranked as dendrimer > gold > other materials. In addition, the active-targeting NPs had higher tumor delivery efficiency than passive-targeting ones (Median: 0.79% vs 0.61%ID; $P = 0.015$). Regarding cancer types, the tumor delivery efficiency was not significant for most types of cancer except that the tumor DE for the liver tumor model was a little lower than that for skin tumors (Median: 0.43% vs 1.23%ID; $P = 0.020$). In the unit of %ID/g tumor tissue, only the variables of the core material, targeting strategy, cancer type, zeta potential, and surface charge were significant for the tumor delivery efficiency. The Dwass−Steel−Critchlow−Fligner (DSCF) tests were performed for significant categorical predictors, which depicted dendrimer NPs (Median: 11.45%ID/g) had higher delivery efficiencies than other ONMs (Medians: 1.88%−3.41%ID/g, Table S3). Active-targeting NPs had a higher delivery efficiency than passive-targeting NPs (Median: 4.12% vs 3.11%ID/g, $P = 0.031$). Considering tumor type, the DE in ovarian tumors (Median: 1.08%ID/g) was significantly lower than those in some other tumors, including breast (Median: 3.49%ID/g), brain (Median: 3.64%ID/g), cervical (Median: 6.18%ID/g), pancreatic (Median: 4.22%ID/g), colon (Median: 3.10%ID/g), and liver (Median: 3.41%ID/g) tumors. The difference between skin and liver tumors was statistically insignificant. The DE of the neutral NPs was significantly higher than the NPs with a negative surface charge (Median: 4.00% vs 2.34%ID/g, $P = 0.001$).

Similarly, multiple variables had significant effects on the tumor C_{max} (PK Parameter #2) in the unit of %ID, including NP type, core material, targeting strategy, cancer type, tumor model, log(HD), zeta potential, and surface charge, while only a few remained significant in the unit of %ID/g tumor tissue, including core material, cancer type, zeta potential, and surface charge. In the unit of %ID, the pairwise comparisons showed that the tumor C_{max} of INMs was comparable to that of hybrid NPs but significantly higher than that of ONMs ($P = 0.003$; Table S3). Among inorganic materials, there were no significant differences between different types of INMs. For core materials, the C_{max} for dendrimers (Median: 9.32%ID) was higher than that of all other organic materials (Median: 0.44%−0.92%ID) and certain inorganic materials, including gold NPs (Median: 1.97%ID, $P = 0.043$), silica NPs (Median: 0.75%ID, $P = 0.008$), and other inorganics (Median: 1.06%ID, $P = 0.003$). For surface charge, the tumor C_{max} for negative NPs was lower than those for positive NPs and neutral ones (Medians: 0.73% vs 1.57% vs 1.22%ID), which is consistent with the findings from tumor DE. For tumor cell lines, the C_{max} in gliomas (Median: 0.07%ID) was significantly lower than that in skin (Median: 2.08%ID) ($P = 0.024$) and cervical tumors (Median: 1.54%ID) ($P = 0.153$). In the unit of %ID/g tumor tissue, the dendrimer NPs (Median: 14.22%ID/g) were delivered to tumors substantially more than other NPs, such as liposomes (Median: 2.91%ID/g, $P = 0.004$), polymeric NPs (Median C_{max}: 4.97%ID/g, $P = 0.011$), and gold NPs (Median: 4.41%ID/g, $P = 0.028$). Consistent with AUC-based tumor DE, the C_{max} in ovarian tumors (Median: 2.32%ID/g) was lower than other tumors based on the unit of %ID/g tumor tissue, including breast (Median: 4.96%ID/g, $P = 0.035$), brain (Median: 4.89%ID/g, $P = 0.016$), cervical (Median: 7.93%ID/g, $P < 0.001$), pancreatic (Median: 5.29%ID/g, $P = 0.017$), colon (Median: 6.10%ID/g, $P = 0.006$), and liver (Median: 4.77%ID/g, $P = 0.019$; Table 1 and Table S3) tumors.

Regarding the tumor distribution coefficient, more variables were significant than the DE and C_{max} using the unit of %ID, including NP type, core material, targeting strategy, cancer type, tumor model, shape, log(HD) (or HD category), and surface charge (Table S4). Regarding core materials, the ONMs had a lower tumor distribution coefficient than hybrid NPs (Median: 0.17 vs 0.65, $P = 0.026$; Table S3). Among different types of NPs, the tumor distribution coefficient was the highest for gold NPs (median: 0.69) and the lowest for liposomes. For ONMs, the tumor distribution coefficient of liposomes (Median: 0.04) was significantly lower than those of hydrogels (Median: 0.26, $P = 0.047$) and polymeric NPs (Median: 0.17, $P = 0.008$). The tumor distribution coefficient for the NPs with passive targeting was lower than those with active targeting (Median: 0.18 vs 0.25). In terms of surface charge, the tumor distribution coefficient (%ID) for positively charged NPs was higher than negative and neutral NPs (Medians: 1.83 vs 0.26 vs 0.11). The tumor distribution coefficient based on the data in the unit of %ID for plate-shaped NPs was lower than that for rod- or spherical-shaped NPs (Median: 0.12 vs 0.18 vs 0.34). For tumor types, the distribution coefficient was lower in colon cancer (Median: 0.05) than for breast (Median: 0.17, $P = 0.031$), brain (Median: 0.30, $P = 0.021$), skin (Median: 1.07, $P < 0.001$), and liver (Median: 0.23, $P = 0.006$) tumors. Using the concentration data in the unit of %ID/g tumor tissue, there were fewer physicochemical parameters significantly affecting the tumor distribution coefficient, including NP type, core material, targeting strategy, and surface charge. The INMs and hybrid NPs had a higher median of distribution coefficient in tumor than the ONMs (1.18 vs 2.08 vs 0.92). In the ONMs, the tumor distribution coefficient was ranked as follows: hydrogel > dendrimer > polymer > liposome. The tumor model and cancer type were also significant predictors of the tumor distribution coefficient. Compared to colon cancer (Median: 0.44), the distribution coefficients to liver tumors (Median: 1.59, $P = 0.002$) and brain tumors (Median: 2.17, $P = 0.022$) were much higher.

In the pairwise comparisons for all PK parameters, gold NPs were highlighted with higher delivery than other materials, which supports the application of gold NPs in cancer diagnostics and therapeutics.[111,112] Based on PK Parameters #1 and #2, the median tumor delivery was ranked as dendrimer > gold > other materials. However, based on PK Parameter #3 of the tumor distribution coefficient, the difference between dendrimers and gold NPs was not significant when the blood PK profiles were taken into consideration. In contrast, the tumor delivery in liposomes was lower than that in other materials regardless of which PK parameters were used, particularly when blood PK was considered in PK Parameter #3. This finding is surprising as liposomes are one of the most commonly used types of NPs in biomedical sciences, including in cancer therapeutics.[113] One of the potential reasons is the

https://doi.org/10.1021/acsnano.3c04037
ACS Nano 2023, 17, 19810−19831

Table 2. Multivariable Linear Regression Analysis Results for the Log-Transformed Pharmacokinetic Parameters[a]

NP	Model	Formula	Sample Size	R^2	Adj. R^2	*P*-value	AIC	BIC
PK Parameter #1: DE (in the unit of %ID)								
All	Full model	Y ~ (Type + MAT + TS + CT + TM + Shape + log (HD) + PDI + ZP)	534	0.308	0.211	<0.001***	553	672
All	Best model	Y ~ (MAT + CT + Shape + log (HD) + PDI + ZP)	534	0.297	0.213	<0.001***	545	643
ONMs	Full model	Y ~ (MAT + TS + CT + TM + Shape + log (HD) + PDI + ZP)	358	0.244	0.141	<0.001***	462	547
ONMs	Best model	Y ~ (MAT + TS + CT + Shape + log (HD) + ZP)	358	0.245	0.184	<0.001***	618	707
Polymeric	Full model	Y ~ (TS + CT + TM + Shape + log (HD) + PDI + ZP)	213	0.234	0.105	0.029*	252	312
Polymeric	Best model	Y ~ (TS + CT + TM + Shape + log (HD) + ZP)	213	0.232	0.136	0.002**	314	380
INMs	Full model	Y ~ (MAT + TS + CT + TM + Shape + log (HD) + PDI + ZP)	160	0.825	0.591	0.008**	60	98
INMs	Best model	Y ~ (MAT + CT + TM + log (HD) + PDI)	160	0.798	0.626	<0.001***	62	93
Gold	Full model	Y ~ (TS + CT + TM + Shape + log (HD) + PDI + ZP)	70	0.861	0.670	0.021*	36	51
Gold	Best model	Y ~ (TS + CT + log (HD) + PDI)	70	0.842	0.727	0.002**	28	38
PK Parameter #1: DE (in the unit of %ID/g)								
All	Full model	Y ~ (Type + MAT + TS + CT + TM + Shape + log (HD) + PDI + ZP)	534	0.226	0.117	0.002**	539	658
All	Best model	Y ~ (MAT + TS + CT + Shape + log (HD) + PDI + ZP)	534	0.223	0.126	<0.001***	529	631
ONMs	Full model	Y ~ (MAT + TS + CT + TM + Shape + log (HD) + PDI + ZP)	358	0.203	0.094	0.011*	449	535
ONMs	Best model	Y ~ (MAT + CT + Shape + log (HD) + ZP)	358	0.205	0.144	<0.001***	590	675
Polymeric	Full model	Y ~ (TS + CT + TM + Shape + log (HD) + PDI + ZP)	213	0.333	0.221	<0.001***	226	286
Polymeric	Best model	Y ~ (CT + TM + Shape + PDI + ZP)	213	0.336	0.246	<0.001***	251	307
INMs	Full model	Y ~ (MAT + TS + CT + TM + Shape + log (HD) + PDI + ZP)	160	0.793	0.517	0.021*	57	95
INMs	Best model	Y ~ (MAT + TS + CT + TM + log (HD) + PDI)	160	0.776	0.564	0.004**	56	88
Gold	Full model	Y ~ (TS + CT + TM + Shape + log (HD) + PDI + ZP)	70	0.802	0.529	0.068	35	50
Gold	Best model	Y ~ (TS + CT + TM + log (HD) + PDI)	70	0.800	0.578	0.033*	30	42
PK Parameter #2: C_{max} (in the unit of %ID)								
All	Full model	Y ~ (Type + MAT + TS + CT + TM + Shape + log (HD) + PDI + ZP)	534	0.307	0.210	<0.001***	545	664
All	Best model	Y ~ (MAT + CT + Shape + log (HD) + PDI + ZP)	534	0.299	0.2116	<0.001***	536	634
ONMs	Full model	Y ~ (MAT + TS + CT + TM + Shape + log (HD) + PDI + ZP)	358	0.249	0.147	<0.001***	456	542
ONMs	Best model	Y ~ (MAT + Shape + log (HD) + PDI)	358	0.203	0.171	<0.001***	446	480
Polymeric	Full model	Y ~ (TS + CT + TM + Shape + log (HD) + PDI + ZP)	213	0.207	0.074	0.081	244	304
Polymeric	Best model	Y ~ (TS + CT + TM + Shape + log (HD) + PDI + ZP)	213	0.218	0.121	0.004**	311	377
INMs	Full model	Y ~ (MAT + TS + CT + TM + Shape + log (HD) + PDI + ZP)	160	0.842	0.630	<0.001***	57	95
INMs	Best model	Y ~ (MAT + CT + TM + log (HD) + PDI)	160	0.811	0.650	<0.001***	60	91
Gold	Full model	Y ~ (TS + CT + TM + Shape + log (HD) + PDI + ZP)	70	0.881	0.716	0.013*	32	47
Gold	Best model	Y ~ (TS + CT + PDI + ZP)	70	0.864	0.752	0.002**	28	39
PK Parameter #2: C_{max} (in the unit of %ID/g)								
All	Full model	Y ~ (Type + MAT + TS + CT + TM + Shape + log (HD) + PDI + ZP)	534	0.211	0.101	0.005**	527	646
All	Best model	Y ~ (MAT + TS + CT + Shape + log (HD) + PDI + ZP)	534	0.208	0.110	0.002**	518	620
ONMs	Full model	Y ~ (MAT + TS + CT + TM + Shape + log (HD) + PDI + ZP)	358	0.195	0.085	0.018*	441	527
ONMs	Best model	Y ~ (MAT + CT + Shape + log (HD) + ZP)	358	0.189	0.127	<0.001***	578	663
Polymeric	Full model	Y ~ (TS + CT + TM + Shape + log (HD) + PDI + ZP)	213	0.286	0.166	0.003**	210	271
Polymeric	Best model	Y ~ (TS + CT + TM + PDI + ZP)	213	0.315	0.229	<0.001***	238	292
INMs	Full model	Y ~ (MAT + TS + CT + TM + Shape + log (HD) + PDI + ZP)	160	0.796	0.524	0.019*	54	92
INMs	Best model	Y ~ (MAT + TS + CT + TM + log (HD) + PDI)	160	0.778	0.568	0.003**	54	87
Gold	Full model	Y ~ (TS + CT + TM + Shape + log (HD) + PDI + ZP)	70	0.796	0.516	0.074	32	47
Gold	Best model	Y ~ (TS + CT + PDI + ZP)	70	0.766	0.575	0.030*	27	39
PK Parameter #3: Distribution Coefficient (based on the concentration data in the unit of %ID)								
All	Full model	Y ~ (Type + MAT + TS + CT + TM + Shape + log (HD) + PDI + ZP)	343	0.411	0.292	<0.001***	424	529
All	Best model	Y ~ (MAT + CT + TM + Shape + log (HD) + PDI + ZP)	343	0.403	0.288	<0.001***	420	515
ONMs	Full model	Y ~ (MAT + TS + CT + TM + Shape + log (HD) + PDI + ZP)	238	0.443	0.340	<0.001***	356	431
ONMs	Best model	Y ~ (MAT + CT + Shape + log (HD) + PDI)	238	0.407	0.325	<0.001***	357	417
Polymeric	Full model	Y ~ (TS + CT + TM + Shape + log (HD) + PDI + ZP)	145	0.514	0.418	<0.001***	196	246
Polymeric	Best model	Y ~ (CT + TM + log (HD) + PDI + ZP)	145	0.506	0.429	<0.001***	191	233
INMs	Full model	Y ~ (MAT + TS + CT + TM + Shape + log (HD) + PDI + ZP)	94	0.856	0.280	0.380	35	56
INMs	Best model	Y ~ (MAT + CT + PDI)	94	0.828	0.670	0.004**	22	37
Gold	Full model	Y ~ (TS + CT + TM + Shape + log (HD) + PDI + ZP)	43	0.899	−0.107	0.685	24	31
Gold	Best model	Y ~ (CT + PDI)	43	0.875	0.786	0.005**	13	16
PK Parameter #3: Distribution Coefficient (based on the concentration data in the unit of %ID/g)								

https://doi.org/10.1021/acsnano.3c04037
ACS Nano 2023, 17, 19810−19831

Table 2. continued

NP	Model	Formula	Sample Size	R^2	Adj. R^2	*P*-value	AIC	BIC
All	Full model	Y ~ (Type + MAT + TS + CT + TM + Shape + log (HD) + PDI + ZP)	343	0.376	0.25	<0.001***	390	495
All	Best model	Y ~ (MAT + CT + TM + Shape + log (HD) + PDI + ZP)	343	0.371	0.25	<0.001***	386	480
ONMs	Full model	Y ~ (MAT + TS + CT + TM + Shape + log (HD) + PDI + ZP)	238	0.446	0.344	<0.001***	321	396
ONMs	Best model	Y ~ (MAT + CT + TM + Shape + log (HD) + PDI + ZP)	238	0.446	0.348	<0.001***	320	391
Polymeric	Full model	Y ~ (TS + CT + TM + Shape + log (HD) + PDI + ZP)	145	0.575	0.491	<0.001***	162	212
Polymeric	Best model	Y ~ (CT + TM + log (HD) + PDI + ZP)	145	0.574	0.496	<0.001***	160	208
INMs	Full model	Y ~ (MAT + TS + CT + TM + Shape + log (HD) + PDI + ZP)	94	0.813	0.067	0.522	35	56
INMs	Best model	Y ~ (MAT + TS + CT + PDI)	94	0.814	0.612	0.014*	21	38
Gold	Full model	Y ~ (Type + MAT + TS + CT + TM + Shape + log (HD) + PDI + ZP)	43	0.858	−0.557	0.771	24	31
Gold	Best model	Y ~ (CT + PDI)	43	0.856	0.752	0.007**	10	14

[a]***$P < 0.001$, ** $P < 0.01$, and * $P < 0.05$. R^2: coefficient of determination; Adj-R^2: adjusted R^2; AIC: Akaike information criterion; BIC: Schwarz Bayesian information criterion; Type: nanoparticle type (inorganic, organic or hybrid NPs); MAT: core material; TS: targeting strategy; CT: cancer type; TM: tumor model; log(HD): log-transformed hydrodynamic size; ZP: zeta potential; DE: delivery efficiency; PK: pharmacokinetic.

limitations of liposomes, including relatively large particle size and shorter systemic circulation period of less than 24 h.[114,115] Additionally, while more than 1000 articles about liposomes and tumors were published every year since 2017,[115] there were 33 studies with 48 data sets that met our inclusion criteria and were included in our analysis. Among these 48 data sets, 46 of the data sets used the encapsulation method to load the drug (the rest are NP only or have no clear statement of the drug loading strategy). Therefore, it is possible that liposome-based nanomedicines do a better job of protecting the drug during the systemic circulation, leading to their better clinical translation despite a lower delivery.

In terms of surface charge, our analysis suggests that neutral and positively charged NPs had a higher tumor delivery than negatively charged NPs. This finding is consistent with our earlier study.[9] Unlike the results of DE and C_{max}, which suggested that the delivery in the positive NPs and neutral NPs were comparable, the delivery measured by PK Parameter #3 showed a significantly higher tumor distribution coefficient for positive NPs than for neutral ones. Mechanistically, positive NPs can be effectively internalized by cells through electrostatic interactions since cell plasma membranes are negatively charged.[116] In a previous study, positive-charged NPs exhibited shorter blood circulation than neutral ones.[117] Since the tumor distribution coefficients were calculated based on the ratios of AUC between tumor and blood, the shorter blood circulation time might be a potential reason that the distribution coefficient of positive-charged NPs became higher than that of other NPs. A mixed effect of surface charge on NP tumor delivery was previously reported.[118] In one study, neutral NPs were suggested to diffuse faster than other NPs because positive-charged and anionic NPs can form aggregates with opposite charge components of the matrix.[119] Some special negative-charged NPs with larger size (~100 nm) were more likely to enter cells through caveolae-independent pathways.[116,118] Overall, the relationship between the surface charge and the tumor delivery of NPs has not been fully understood. More mechanistic studies need to be conducted on this topic, but caution must be taken to identify what PK parameters are used.

In addition, we assessed the impact of the administrative dose on tumor delivery to examine whether there is a threshold of the dose to achieve maximum tumor delivery. According to the correlation and linear regression results, there was not a significant linear relationship between the administration dose to tumor-bearing mice and the tumor delivery (Figure S5). The correlations were also very small using different PK parameters in different units (Table S5). However, the ANOVA analyses and pairwise comparisons of the tumor delivery in dose groups suggested that the tumor delivery may have a bell-shaped curve in which the tumor delivery achieved the peak at the dose group 10° (i.e., the dose ranges from 1 to 9.9 mg/kg) (Figures S6 & S7, Tables S6 & S7). Such a threshold did not exist using PK Parameter #3 of the distribution coefficient (Figures S8 & S9, Tables S8 & S9). Overall, our results suggest that there may be a threshold-like dose of 10 mg/kg to maximize the tumor DE based on PK Parameter #1 (i.e., the traditional method of representing tumor DE). Higher administration doses beyond this value may not increase the tumor DE in the tumor-bearing mice. In the study by Ouyang et al. (2020),[120] they derived a dose threshold for NP tumor delivery of 1 trillion NPs. Since our study and the Ouyang et al. study[120] used different units and were based on different data sources, it is difficult to compare our results. However, assuming an average molecular weight of 5000 kDa for NPs and an average mouse body weight of 20 g, a dose of 1 trillion NPs can be converted to 0.01 mg/kg, which is actually below the most administration doses in our selected studies as well as our results of the dose threshold. Nevertheless, our study and the study by Ouyang et al. (2020)[120] together suggest the existence of a threshold-like dose for NP tumor delivery to achieve the maximum delivery efficiency. Further studies are needed to derive a more precise threshold dose value for different types of NPs with different units.

Subgroup Multivariable Linear Regressions of Tumor Delivery. Multivariable linear regressions were performed to assess the log-transformed subgroups of NPs, including gold NPs, polymeric NPs, INMs, ONMs, and all NPs. In total, we report 60 regression models from 3 log-transformed PK parameters (DE, C_{max}, and distribution coefficient) based on the concentration data in two units (%ID and %ID/g tissue). For each PK parameter, we included both full (i.e., the full model including all testing variables) and best (i.e., the best subset model with the highest adjusted R^2 and lowest AIC/BIC values) models for all NP subgroups.

The results of multivariable linear regression are listed in Table 2 and Table S10. In Table 2, we performed the analyses

https://doi.org/10.1021/acsnano.3c04037
ACS Nano 2023, 17, 19810−19831

with the original data of the zeta potential (i.e., as a continuous variable), while in Table S10, we explored the use of surface charge as a categorized variable based on the zeta potential to investigate whether categorized physicochemical parameters can better predict the tumor DE of NPs.

Based on the continuous variable zeta potential, the best regression models describing the tumor DE based on all 534 data sets using PK Parameter #1 of tumor DE in the unit of %ID were: all NPs (R^2 = 0.297, P < 0.001), ONMs (R^2 = 0.245, P < 0.001), INMs (R^2 = 0.798, P < 0.001), polymeric NPs (R^2 = 0.232, P = 0.002), and gold NPs (R^2 = 0.842, P = 0.002) (Table 2). The key predictors included cancer type, log-transformed hydrodynamic size, and PDI for all groups. Zeta potential and shape were also significant factors for the organic NPs, including the group of ONMs and the group of polymeric NPs as well as the composite group in which the proportion of the ONMs data was 67%. The regression results of PK Parameter #2 C_{max} were similar to the results of PK Parameter #1 DE with a similar goodness of fit and key predictors in both units.

Taking the blood PK profile into account, for inorganic NPs, the regression models of the distribution coefficient demonstrated a high but similar goodness of fit with physicochemical and experimental variables (R^2 > 0.8) compared to the other two parameters, tumor DE and C_{max}. For organic NPs, compared to DE and C_{max}, the distribution coefficient (%ID) improved the R^2 for the composite group of all NPs (R^2 = 0.403, P < 0.001 vs R^2 = 0.297 (DE) vs R^2 = 0.299 (C_{max})), ONMs (R^2 = 0.407, P < 0.001 vs R^2 = 0.245 (DE) vs R^2 = 0.203 (C_{max})), and polymeric NPs (R^2 = 0.506, P < 0.001 vs R^2 = 0.232 (DE) vs R^2 = 0.218 (C_{max})). Similar results were derived based on the concentration data in the unit of %ID/g. Besides, the regression with surface charge showed comparable results with zeta potential (Table S10). We used the results with the original data of the zeta potential (Table 2) for further discussion and drew the conclusions of this study as described below.

Since different physicochemical properties affected the tumor delivery of different types of NPs differentially, we also presented the specific regression coefficient values (i.e., positive impact or negative impact) and prediction profilers of significant physicochemical properties on tumor DE in the unit of %ID of all NPs, INMs, ONMs, and gold NPs based on the best multivariate regression model results. The results are presented in Section 2 of the Supporting Information. Ultimately, one potential application of our regression models is to determine what combinations of parameters may lead to a higher tumor DE. To illustrate this application, we applied our best multivariate regression models to generate several hypothetical scenarios of different combinations of NP factors for 1000 iterations, and representative scenarios that had a relatively higher tumor DE of >3%ID or even >5%ID are presented in Tables S11–S14. For example, gold NPs with features of hydrodynamic size between 10 and 100 nm, active targeting, and a low PDI may achieve a DE exceeding 5%ID in skin, breast, ovary, prostate, and other cancers (Table S14). We note that these are hypothetical simulated scenarios, which will need further experimentation to confirm.

Nanoparticle Biodistribution in Main Organs. In addition to the evaluation of tumor delivery, we summarized NP biodistribution in the major healthy organs, including heart, liver, spleen, lung, and kidney, and simultaneously assessed the relation between the physicochemical factors and NP biodistributions in these major healthy organs and tumors. This analysis was performed to evaluate the impact of the distribution to major healthy organs on NP tumor delivery. The organ distributions of NPs are summarized in Figures 5 &

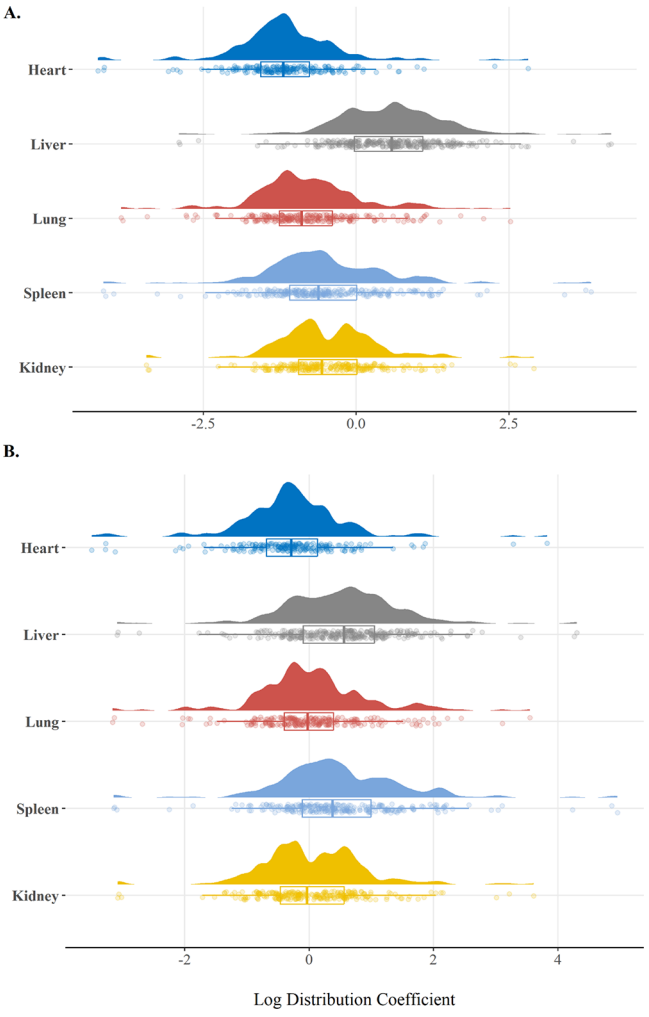

Figure 5. Summary of nanoparticle (NP) biodistributions in the major organs. The biodistribution is presented with distribution coefficient calculated with the data in the unit of (A) %ID and (B) %ID/g tissue. The spots under each biodistribution curve showed the individual biodistribution data of each NP from each data set. The box indicates the 50th percentile interval from the 25th to 75th percentile estimate; the whisker indicates the 95th percentile interval from 2.5% to 97.5%.

S10–S13. Using the parameter of DE (PK Parameter #1), the median biodistributions of NPs were as follows: heart: 0.19%ID (95% CI: 0.002% – 5.52%ID), lung: 0.33%ID (95% CI: 0.005% – 8.31%ID), spleen: 0.66%ID (95% CI: 0.009% – 13.30%ID), kidney: 0.97%ID (95% CI: 0.017% – 14.59%ID), and liver: 11.25%ID (95% CI: 0.17% – 75.98%ID) (Figure S10).

The MANOVA results suggested that the NP type, core material, targeting strategy, cancer type, tumor model, shape, hydrodynamic size, and surface charge all contributed to the distribution differences among organs. For each organ, the key predictors are different. For example, the liver accumulation was affected by many factors including NP type, core material, cancer type, tumor model, shape, and size, while the heart

https://doi.org/10.1021/acsnano.3c04037
ACS Nano 2023, 17, 19810–19831

Table 3. Multivariate and Univariate Associations of Physicochemical Characteristics with Organ Biodistribution Presented as Distribution Coefficient (Parameter #3) Based on the Concentration Data in the Unit of %ID[a]

	Organs					
	Heart	Liver	Spleen	Kidney	Lung	*P*-value
Nanoparticle Type	0.434	0.270	0.025*	0.625	0.416	0.037*
Core Materials	0.064	0.005**	<0.001***	<0.001***	0.029*	<0.001***
Targeting Strategy	0.859	0.984	0.969	0.229	0.970	0.275
Cancer Type	<0.001***	0.002**	<0.001***	0.001**	<0.001***	<0.001***
Tumor Model	0.952	0.936	0.568	0.926	0.620	0.023*
Shape	0.088	<0.001***	<0.001***	0.079	0.005**	<0.001***
Size	0.093	0.023*	0.014	0.118	0.021*	<0.001***
Surface Charge	0.254	0.338	0.295	0.109	0.301	0.148

[a]The result of this table is presented as distribution coefficient (Parameter #3) based on the concentration data in the unit of %ID. The results based on other methods using different units are presented in Tables S15−S19 in Supporting Information. ***$P < 0.001$, **$P < 0.01$, and *$P < 0.05$. Size: log-transformed hydrodynamic size.

accumulation was only affected by core material, cancer type, tumor model, size, and surface charge (Table S15). In terms of liver accumulation, the ONMs had less distribution than INMs (Median: 8.90% vs 16.01%ID, $P < 0.001$) and hybrid NPs (Median: 8.90% vs 22.54%ID, $P = 0.042$). Rod-shaped NPs were more likely to accumulate in the liver compared to other shapes, particularly compared to spherical NPs (Median: 24.81% vs 10.19%ID, $P = 0.001$). Moreover, the effects of hydrodynamic size on accumulation in the liver showed a significant positive correlation, with larger NPs being more likely to accumulate. Compared to the NPs less than 10 nm, the liver distributions were relatively high for those in 10−100 nm (Median: 4.50% vs 11.89%ID, $P = 0.003$), those in 100−200 nm (Median: 4.50% vs 10.72%ID, $P = 0.107$), and those larger than 200 nm (Median: 4.50% vs 16.60%ID, $P = 0.002$). The difference between the groups of 10−100 and 100−200 nm was not significant (11.89% vs 10.72%ID, $P = 0.197$). A similar effect of size was found in heart accumulation, with the NPs less than 10 nm having the least accumulation (Median: 0.07%ID for <10 nm vs 0.22%ID for 10−100 nm vs 0.15%ID for 100−200 nm vs 0.31%ID for >200 nm). In contrast, the effects of NP type and shape were not significant on heart accumulation.

Considering organ weights, the biodistributions were heart: 1.52%ID/g (95% CI: 0.012% − 46.45%ID/g), lung: 2.44%ID/g (95% CI: 0.04% − 63.67%ID/g), kidney: 3.22%ID/g (95% CI: 0.05% − 51.04%ID/g), spleen: 6.93%ID/g (95% CI: 0.10% − 127.85%ID/g), and liver: 10.69%ID/g (95% CI: 0.16% − 75.01%ID/g) (Figure S11). The significant predictors were the same as those for the unit of %ID except for the surface charge, which was barely significant ($P = 0.078$). The pairwise comparison results were similar to those based on the concentration unit of %ID. For example, the ONMs accumulated less than INMs (Median: 8.56% vs 15.44%ID/g, $P < 0.001$) and hybrid NPs (Median: 8.56% vs 22.25%ID/g, $P = 0.048$) in the liver. Polymeric NPs had a lower liver accumulation than gold NPs (Median: 7.11% vs 18.43%ID/g, $P = 0.034$).

The organ biodistribution trends were similar for the results based on the other two PK parameters of C_{max} and the distribution coefficient, in which NP accumulation was significantly higher in the liver than other organs, followed by the spleen and the kidney. The significant predictors for each PK parameter are listed in Tables 3 & S15−S19. Using the parameter of distribution coefficient calculated using the data in the unit of %ID, the heart accumulation for the NPs was only different with cancer types, indicating the difficulty to predict the heart accumulation of NPs by using physicochemical parameters and study design factors compared to other organs. The results of higher accumulation in the liver than other organs are consistent with the observation in healthy animals.[16,87,121] This result showed competition between the RES system (e.g., liver and spleen) and the tumor for distribution of NPs.

Mechanistically, liver, spleen, and kidney are the main accumulative organs for NPs regardless of exposure routes, animal models, and physicochemical properties of NPs.[122] The effects of physicochemical parameters on organ biodistribution are more complicated than those on tumor delivery, because organs are more differentiated and functionalized and generally have highly regulated blood flows. As the hydrodynamic diameters of most current NP designs are within 10−200 nm, the main excretion route for these NPs is via feces.[123] Additionally, the fenestrations in the endothelial cells in the liver allow for relatively larger (compared to the NPs mainly cleared in the renal system) foreign particles such as NPs, to be trapped in a manner similar to the enhanced permeability and retention (EPR) effect, which partially contributes to the nonspecific accumulation of NPs within the liver.[124,125] Several studies have shown that the majority of nonspecific accumulation of NPs in the liver is due to Kupffer cells.[109,125,126] In a review of NP-liver interactions, the liver was estimated to sequester 30%−99% of administered NPs from the bloodstream.[127]

As another important component of the RES system, the spleen was shown to also significantly contribute to the removal of NPs. In our study, the amount of NP in the spleen was comparable to that in the kidney. In a study by Tsoi et al.,[125] significant uptakes of NPs by splenic macrophages were found, which, however, were still lower than Kupffer cells in the liver.[125] Taveres et al. (2017) found compensatory increases of gold NP intake in the spleen after removing Kupffer cells in tumor-bearing mice.[128] Besides, the ultrasmall NPs with a size <8 nm can be excreted via the urine.[129] Therefore, many ultrasmall NPs will have access to renal tissue and may produce higher kidney accumulation.[130,131] However, high renal clearance of these ultrasmall NPs does not always coincide with high kidney retention or accumulation, since they can be quickly cleared into urine. For example, 5 nm Ng gold composite nanodevice ($(Au^0)_{6.45}$-PAMAM_E4.5-$(COOH)_{64}$: 5 nm Ng-Au-CND) had a kidney biodistribution of 2.75%ID at 24 h, whereas the liver accumulation was 22.1%

https://doi.org/10.1021/acsnano.3c04037
ACS Nano 2023, 17, 19810−19831

ID at the same time point.[132] In contrast, high kidney accumulation can occur with some large NPs (>10 nm) having certain characteristics. In our database, Kanazaki et al. (2015)[133] developed antibody-conjugated iron oxide NPs (antiepidermal growth factor receptor 2 (HER2) scFv-conjugated IONPs-20 nm: SNP20) and found comparable accumulation in the liver and kidney at 24 h (10.6 vs 22.9%ID/g). In the ANOVA results of liver biodistribution, the significant factors affecting the distribution of NPs included the use of the cancer cell line and core material for all PK parameters.

Future efforts on the design of NPs need to consider the competitive effects of organs with tumors in systemic circulation and tissue distribution.[109] The more NPs that are trapped by nontumor cells, the lower tumor delivery efficiency will be. To enhance tumor delivery, future NP designs can improve certain NP properties to reduce potential accumulation in healthy tissues or even the toxicity of NPs, which would reduce the competition and thus increase NP tumor delivery.

Strengths and Limitations of the Current Study Compared to Existing Relevant Studies. Compared to our earlier version of the "Nano-Tumor Database",[9] the present study increased the number of tumor time-dependent concentration data sets from 376 to 534 and increased the number of tumor concentration data points from 1381 to 2345, adding 97 studies published between 2018 and 2021 (Table 4). The current database also added 1972 data sets in several major healthy organs (340 data sets for heart, 456 for liver, 367 for lung, 413 for spleen, and 396 for kidney) with a total of 8461 concentration data points, which were not available in the previous version of the database, enabling us to provide a comprehensive analysis on the whole body biodistribution as well as tumor delivery of different NPs. Moreover, we calculated the PK parameters based on the concentration data in two units: %ID and %ID/g tissue. Typically, the delivery efficiency is expressed in the unit of %ID. However, as the tumor sizes differ between different studies, it may not be accurate to measure the NP disposition in tumors without considering the tumor size and weight. Therefore, the units of %ID and %ID/g tissue were used to represent the absolute distribution to individual organs and the relative distribution among different organs, respectively. Tumor delivery could be quite different using different units.

Besides substantially increasing the type and size of the "Nano-Tumor Database", another strength of the present study is the use of multiple PK parameters to simultaneously evaluate the NP delivery to the tumor and major healthy organs as well as interpret the impacts of physiochemical properties and experimental conditions. Traditionally, the AUC-based DE is usually used to assess the NP delivery to tumor. For example, Wilhelm et al. (2016) analyzed the tumor DE studies of NPs from 2005 to 2015 and derived a median DE of 0.7%ID to a solid tumor.[5] Cheng et al. (2020) also predicted the tumor DE of different NPs using a PBPK method based on AUC-based %ID with a comparable result.[9] Using the same method, we also yielded a median AUC-based tumor DE (%ID) of 0.67%ID. Besides, we calculated and compared the tumor delivery using two other PK parameters, C_{max} and distribution coefficient, which was defined as the AUC ratio between the target tissue and blood.

It should be noted that each PK parameter has its own strengths and limitations for the evaluation of NP delivery and

Table 4. Differences of the Current Study Compared to Existing Relevant Studies[a]

	Wilhelm et al. (2016)	Price et al. (2020)	Cheng et al. (2020)	Fan et al. (2021)	Current study by Chen et al.
Scope of the data	Tumor only	Tumor only	Tumor only	Tumor and major organs	Tumor, blood, and major organs
Years of the data	2005–2015	2005–2015	2005–2018	2005–2018	2005–021
Number of publications	117	117 (Based on Wilhelm et al. 2016)	200	200 (Based on Cheng et al. 2020)	297
Number of data sets	232 for tumors	256 for tumors	376 for tumors	376 for tumors and 1381 for major organs (heart: 227, liver: 327, lung: 292, spleen: 252, kidney: 283)	534 for tumors and 1972 for major organs (heart: 340, liver: 456; lung: 367, spleen: 413, kidney: 396)
Characteristics of data sets	Single time point and multiple time points	Single time point or multiple time points	At least 3 time points for each data set	At least 3 time points for each data set	At least 3 time points for each data set
Number of data points	NA	NA	1722 for tumors	1732 for tumors and 6039 for major organs	2345 for tumors and 8461 for major organs
Unit of data	%ID	%ID	%ID	%ID and %ID/g	%ID and %ID/g
PK parameters	DE for tumors only	four different parameters for tumors only	DE and the PBPK method	DE for tumors only	DE, C_{max}, and DC for both tumors and major organs
Availability of data	Yes	No	Yes	Yes	Yes

[a]Note: Please refer to the Methods section regarding definitions of pharmacokinetic (PK) Parameter #1 – #3. DE: delivery efficiency; DC: distribution coefficient; NA: not available.

https://doi.org/10.1021/acsnano.3c04037
ACS Nano 2023, 17, 19810–19831

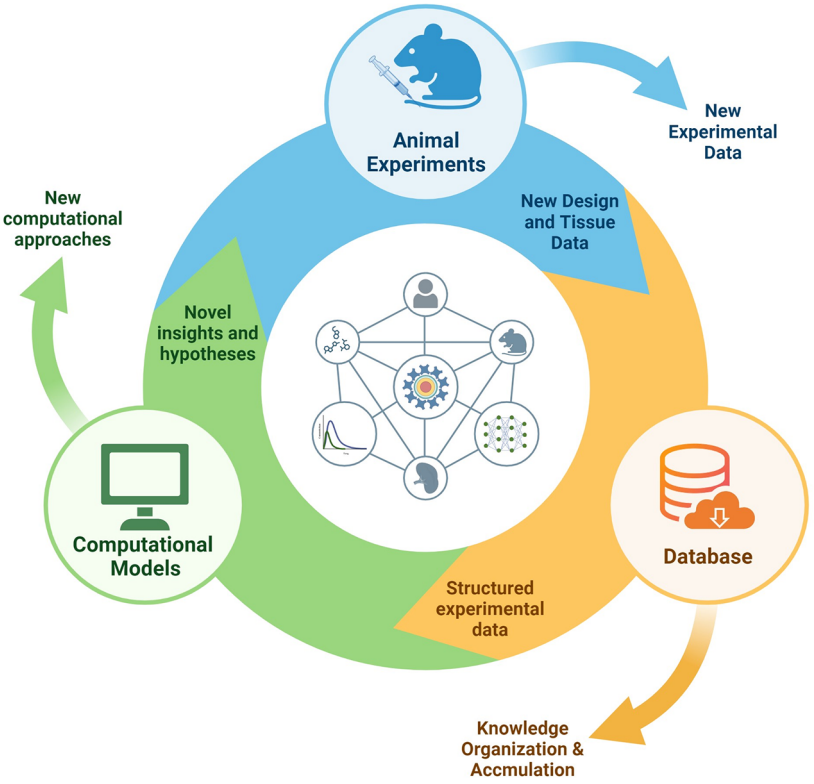

Figure 6. A strategic cycle in facilitating the design of nanoparticles/nanomedicines which consists of animal experiments, databases, and computational models (This figure was created with BioRender.com).

the interpretation of the physiochemical impacts. The advantages of DE and C_{max} have been discussed previously in the literature.[5,10] Regarding the distribution coefficient, it represents a holistic consideration of tumor within the context of the whole body by taking the blood PK profile into account. In the blood, NPs can be bound to plasma proteins to form NP-protein coronas. Formation of NP-protein coronas can alter the PK, biodistribution, and toxicity of NPs.[134,135] Based on various physicochemical properties and different experimental conditions, such as administration route and animal disease state, the NPs can retain the protein corona as a specific "fingerprint".[136] Therefore, protein binding information *in vivo* will be very important to predict the tumor delivery efficiency of NPs and the biodistribution, which warrants further investigation.

Additionally, the information on blood flow dynamics can also be indirectly taken into consideration by including the blood PK profile in our analysis. The tumor DE was suggested to be influenced by the blood flow.[11] The treatment of mild hyperthermia, which can increase tumor blood flow locally, was suggested to enhance the tumor-targeting delivery efficiency of NPs by up to 3-fold.[11] Furthermore, the blood flow speed can vary in different organs and tissues. For example, the velocity of NP travel in arteries and veins can be over 10-fold of that in liver sinusoid, which promotes the NP liver accumulation.[125] Accordingly, when analyzing tumor DE of NPs,[5,9] it may be beneficial to account for the impacts of more biological factors, such as the tumor weight, blood PK profile, and distribution of NPs to healthy organs.

There are some limitations in this study. First, this analysis was based on a few assumptions due to the lack of more granular data. The type of blood collected was not included in the analysis. To calculate the distribution coefficient of the tumor and healthy organs, we categorized blood data as blood, plasma, and serum. In 343 blood data sets, there were 218 data sets for blood, 124 data sets for plasma, and 1 for serum. To address the different volumes of plasma and blood, we used 4.9% and 3.55% for relative blood and plasma volume fractions in the data calculation, respectively.[137] However, the cell-NP interactions in blood cannot be fully addressed due to the lack of cellular reactivity and binding information on NPs. We had to assume that only a limited number of NPs were trapped in the cells and proteins in the blood. The number of NPs in the blood was assumed to be approximately equal to that in the plasma or serum. In the blood or plasma, the formation of biomolecular coronas will substantially affect the PK profile of NPs.[7] In previous studies, the changes in targeting capabilities of NPs were reported to be impacted by the physicochemical properties, such as NP surface modification. Therefore, the PK profiles of NPs will be different in blood and plasma. Thus, we conducted the subgroup multivariable linear regressions using the PK parameter of the distribution coefficient (i.e., the AUC ratio between tumor versus blood and/or plasma). The results suggested that the R^2 for the blood subgroups was higher than the overall results for both all NPs and organic NPs, and the results for the plasma subgroup were also higher than the overall result for all NPs (Table S20). Therefore, the model can be better fitted if the blood composition criteria for the NPs can be included.

Second, the interactions between the dispersive media and NPs were not taken into account. Previous studies have shown that the dispersive media, such as phosphate-buffered saline (PBS), can interact with certain NPs and subsequently change the surface charge and zeta potential of NPs, such as silica NPs and poly(acrylic acid) (PAA)-coated cobalt ferrite NPs.[138] The measured zeta potential for PAA NPs ranged from −14 mV

https://doi.org/10.1021/acsnano.3c04037
ACS Nano 2023, 17, 19810−19831

(RPMI-1640 medium +10% fetal bovine serum (FBS)) to −59 mV (distilled water). In contrast, the silica NPs had relatively stable zeta potential measurements from −1 mV (NaCl) to −10 mV (PBS with 10% FBS). In another study of inorganic NPs including gold, silver, ZnO, Fe_2O_3, and TiO_2 NPs, the measured zeta potentials were different in cell culture media and human serum from the water.[139] In our analysis, most studies used water as the dispersive media, but some studies used other media, such as PBS (pH = 7.4).[17,31] This should be considered a caveat that may limit the validity of our conclusion. Also, it is important to note that this study focuses on the PK of NPs, which is different from the PK of the delivered drug. Further studies are needed to evaluate the delivery efficiency of NPs versus that of the delivered drug.

Third, a potential issue of overfitting in the full models may occur in the analysis of multivariable linear regression due to the number of physicochemical parameters and relatively small sample sizes. Consequently, the linear regression analysis for the INMs and gold NPs may be overfitted using the parameter of distribution coefficient, which caused some negative adjusted R^2 values for the full models (Tables 2 & S10). However, in the best subset regression models, the number of physicochemical properties was reduced, and the adjusted R^2 became positive. For example, using the tumor distribution coefficient (%ID), the adjusted R^2 for the gold NPs was −0.107 for the full model, while it became 0.786 for the best model ($P = 0.005$). We closely examined the extreme values of the delivery efficiency in tumors in the subgroups of INMs and gold NPs using a sensitivity analysis for the methods with negative R^2 values [i.e., tumor distribution coefficient calculated based on the data in the units of %ID and %ID/g, respectively] and the classic method of AUC-based delivery efficiency. The results are presented in Table S21. The R^2 and adjusted R^2 values for the distribution coefficients were not significantly changed. Moreover, using the Rosner's outlier test[10,140] to verify the sensitivity analysis results, the negative adjusted R^2 was not changed by removing the outliers (data not shown). Therefore, the full data sets in our analysis were used, as the results were not affected by potential outliers after a data quality check. More sophisticated machine learning and deep learning algorithms should be considered to build more robust quantitative models to predict tumor delivery efficiency of NPs based on this updated "Nano-Tumor Database".[141,142] Additionally, higher-quality data and more standardized data collection and reporting methods will be helpful for these types of meta-analyses.

Perspective. To apply the data compiled in this study to support nanomedicine research, we propose a long-term strategic cycle to optimize NP design and improve the NPs' DE and efficacy in tumors (Figure 6). Animal experiments are still the fundamental basis and the initial step in the design, DE, efficacy, and safety evaluation of NPs. In animal experiments, tumor delivery, blood or plasma PK, and organ biodistribution data can be generated for different types of NPs. By leveraging animal experimental data, databases containing NPs' physicochemical properties, study design information, and blood/tissue PK data can be compiled in a structurally consistent and comparable format, such as what was done in this and previous studies.[5,9,11] This will make vast experimental data accessible and readily useful to a broader community of researchers in various disciplines for promoting nanomedicine research. With the availability of large databases, computational models and mathematical tools can play a pivotal role in this cycle, not only summarizing the existing knowledge but also developing insights and generating hypotheses, such as the hypothetical scenarios presented in this study (Tables S11−S14). These hypotheses can subsequently be verified or refined through animal experiments, thus creating a productive and iterative cycle that continuously advances nanomedicine research.[143]

Currently, the establishment of the NP databases and utilization for computational modeling approaches are witnessing notable progress. Based on a large number of animal studies, several databases have been developed and continuously updated, including the present study.[5,9,11] Taking advantage of existing databases, there are many studies analyzing the existing data and predicting the *in vivo* fate of NPs by using cutting-edge computational methodologies, such as PBPK modeling and artificial intelligence methods.[9,142,144] However, the application of computational modeling results to inform animal experiments has progressed at a slower pace. Current animal experiments of NP designs have not embraced and capitalized on the insights gained from computational modeling of existing knowledge. This limitation hinders the realization of the full potential of these computational tools for improving NP designs. To overcome this hurdle, we advocate for a more cohesive integration of computational modeling into the design of NPs. As a starting step, we hope the several multivariate regression models (Table 2 and Tables S10 and S20) and the several hypothetical scenarios (Tables S11−S14) presented in this study will help guide animal experimental designs for NPs with a higher tumor DE in the future. We believe this will lead to significant improvements in the physicochemical properties of NPs and ultimately facilitate the clinical translation of nanomedicines.

CONCLUSIONS

In summary, the present study reports an updated version of the "Nano-Tumor Database". This curated database contains 534 data sets on tumor concentrations of different NPs collected from 297 studies published from 2005 to 2021. Each data set has at least three data points (a total of 2345 data points for 534 data sets) so that the data are minimally sufficient to perform a PK analysis. In this updated version of the database, we also collected NP distribution in blood (or plasma) and major healthy organs from each of the studies when available, resulting in 1972 data sets (340 for heart, 456 for liver, 367 for lung, 413 for spleen, and 396 for kidney) and 8461 data points. All data are published as a Supporting Information Excel file with this manuscript and are also available in a public repository in GitHub (https://github.com/UFPBPK/Nano-Tumor-Database-Version2023).

Based on the curated data, we calculated the tumor delivery and organ distribution using three PK parameters based on the concentration data in two different units (%ID and %ID/g tissue). Our study highlights the importance of using a variety of PK parameters to evaluate the tumor delivery of NPs from different perspectives. Notably, the values of these three parameters themselves are not comparable due to different definitions.

Moreover, our multivariate regression analysis suggests that certain physicochemical and experimental factors, such as core material, surface charge, and cancer type, are crucial to predicting the tumor delivery and organ accumulation of NPs. These factors can impact tumor DE indirectly through the influence on organ biodistribution competing with tumor

https://doi.org/10.1021/acsnano.3c04037
ACS Nano 2023, 17, 19810−19831

delivery. Overall, this study improves our understanding of the interaction between NPs and tumors and the effects of the physicochemical properties on tumor DE. Several statistical regression models were established that could be used to predict tumor DE and to help design NPs based on different physicochemical and experimental factors, which may in turn facilitate the NP design in the future and improve the clinical translation in the field of cancer nanomedicine. As an example, we applied our best multivariate regression models to generate several hypothetical scenarios of different combinations of factors that might lead to a relatively higher tumor delivery efficiency of >3%ID or even >5%ID (Tables S11−S14), which will definitely need further experimentation to confirm. We envision that the updated "Nano-Tumor Database" will provide a rich and publicly available data source for other researchers, enabling further computational analysis and fostering advancements in nanomedicine research by facilitating NP design optimization and improving clinical translation from bench work to bedside.

MATERIALS AND METHODS

Data Collection. The processes of searching the literature, screening the papers, and applying the inclusion and exclusion criteria are listed in Figure 1. Briefly, this study included relevant studies published between 1/1/2005 and 6/30/2021. The raw tumor concentration data from studies published between 2005 and 2018 were extracted in an earlier study by Cheng et al. (2020).[9] The studies published between 2018 and 2021 were screened from PubMed with the keywords "nanoparticle delivery" or "nanomaterial delivery", "biodistribution" or "pharmacokinetics", "mice" or "rats", and "tumor" or "tumour". A total of 1345 studies were identified in PubMed. The literature screening consisted of two steps based on the abstract and the manuscript, respectively. Step one was to screen out some studies if they were: (1) retracted papers; (2) reviews or meta-analyses; (3) lack of biodistribution or pharmacokinetics data, or (4) conducted in healthy rodents. Second, by reviewing the entire manuscript, we excluded additional studies if the study (1) contained less than 3 sampling time points; (2) had more than one type of tumor per animal; (3) used other administration routes rather than IV injection; and (4) the percentage of injected dose (%ID) in the tumor could not be calculated based on the data. Finally, we also excluded the rat studies, as most studies were conducted in tumor-bearing mice and the present study was focused on mice. The amount of data in rats was not sufficient for comparison of the tumor delivery efficiency of NPs between different animal models.

Based on the inclusion and exclusion criteria, a total of 158 recent data sets mainly from 97 articles published between 2018 and 2021 were included for analysis in this study.[12−108] For each data set, the relevant parameters of the physicochemical properties of the NPs, including the composition, organic/inorganic materials, targeting strategy, zeta potential measured at pH 7.4, surface chemistry, hydrodynamic diameter, core diameter measured via TEM, PDI, and shape as well as the experimental methods, including tumor model, cancer type, tumor cell type, tumor size, tumor weight, experimental animal, sex, body weight, strain, administration position, administration dose, and the raw NP concentration data in the tumor were collected. Compared to the earlier study by Cheng et al. (2020) that only collected concentration data in tumors,[9] this study also collected the concentration data in the blood and five major organs (heart, liver, spleen, lung, and kidney) to have a more comprehensive understanding of the tissue distribution of NPs in tumor-bearing mice. By adding the 158 recent data sets to the "Nano-Tumor Database" that already contained 376 data sets,[9] there are now 534 data sets on the distribution to tumor and healthy tissues of different NPs from 297 articles.

Biodistribution Data Conversion. To compare data from different articles having different experimental designs and data expressed using different units, the raw concentration data from all studies were collected and converted to the units of %ID and "%ID per gram tissue" (%ID/g). (Detailed methods are provided in Section 1 of the Supporting Information). The density of blood and main organs was assumed to be 1 g/mL, while the density of solid tumors was assumed to be 1.2 g/cm^3.[9] The weights of healthy organs were calculated by multiplying the body weight by a fraction for each organ, which were obtained from the literature and are listed in Table S22. If available, the actual body weight reported in the original articles was used in the calculation. Otherwise, an assumed body weight of 20 g was applied based on earlier studies.[5,9]

Some studies reported the biodistribution data using the concentration of a single element of the components of the NPs, such as the inorganic material of the NP formulation or the loading drug. For example, Bao et al. (2018)[74] reported the biodistribution of the poly(ethylene glycol) (PEG)-modified, platinum-doped, carbon NPs (denoted as PEG-PtCNPs) with the %ID of platinum in tissues. In another instance, Mu et al. (2020)[104] assessed the biodistribution of PEGylated NPs in female BALB/c mice and presented the data using the total drug (paclixel) percentage in the tumor and organs.[104] However, it may not be accurate to use a single element or the loading drug of the NPs to calculate the NP biodistribution in the tumor and organs as well as to compare the results across different studies. In these cases, we applied the method from the Wilhelm et al. study[5] and calculated the administered dose and tissue concentrations of the whole NP formulation using the concentrations of partial components or the loading drug. The details of the dose estimation method are described in the Additional Methods of the Supporting Information. The default values of the parameters are given in Table S22.

Pharmacokinetic Parameter Calculation. After the raw biodistribution data were converted to the units of %ID and %ID/g, tumor delivery and organ distribution of NPs were calculated using three different PK parameters, including (1) delivery efficiency (DE) in the unit of %ID or %ID/g tissue calculated based on AUC (the AUC from t-zero to t-last), (2) the maximum observed NP concentration in a particular tissue (C_{max}), and (3) the tissue/blood distribution coefficient calculated as the AUC ratio of the tissue and blood (AUC_{tissue}/AUC_{blood}).[10]

A summary of the definitions and significance of these three PK parameters is presented in Table 5. Besides involving the classic PK parameter of DE to evaluate tumor delivery and organ biodistribution, the use of C_{max} can be related to the maximum therapeutic effect and potential toxicity, while the distribution coefficient of the target tissue enables the consideration of drug delivery holistically within the organism. When the distribution coefficient is calculated based on the concentration data in the unit of %ID, it assesses the ratio of the total drug amount between the target tissue and the blood, whereas when the distribution coefficient is calculated based on the concentration data in the unit of %ID/g, it can assess the ratio of the drug concentration between the target tissue and the blood.

In PK Parameter #1, AUC-based tumor delivery efficiency was calculated using a noncompartmental linear trapezoidal integration method (Figure 2). The trapezoidal rule is shown with the following equations[5]

$$\mathrm{AUC}_i = \frac{1}{2}(C_{i-1} + C_i) \times (t_{i-1} + t_i) \quad (1)$$

$$\mathrm{AUC} = \sum_{i=1}^{n} \mathrm{AUC}_i \quad (2)$$

$$\text{delivery efficiency} = \mathrm{AUC}/t_i \quad (3)$$

where C_{i-1} and C_i are the corresponding concentrations of the NPs at the time points t_{i-1} and t_i, respectively. According to the units of the corresponding concentrations, the AUC can be expressed in %ID·h or %ID/g·h. Thus, the unit of the delivery efficiency is %ID or %ID/g tissue.

https://doi.org/10.1021/acsnano.3c04037
ACS Nano 2023, 17, 19810−19831

Table 5. Summary of the Pharmacokinetic Parameters Used in This Study for Evaluation of Tumor Delivery and Organ Biodistribution

	Calculation	Significance
Delivery efficiency (DE)	Delivery efficiency = AUC/t where AUC is the area under the curve of the concentration in the target tissue, while t is the last measured time point in the data set. AUC is calculated based on a noncompartmental linear trapezoidal model.	Delivery efficiency is a classical pharmacokinetic parameter to assess the average drug amount or concentration in a particular tissue during the measured period.
C_{max}	The maximum observed concentration in the target tissue which is determined by visual inspection.	C_{max} is a standard measurement in pharmacokinetics to evaluate the maximum concentration that a drug can achieve in the plasma or tissue.
Distribution Coefficient	Distribution coefficient tissue/blood = AUCtissue/AUCblood	Distribution coefficient represents the extent of distribution of a drug or a NP to a tissue relative to the blood. It is a composite parameter that considers the ratio in the amount or concentration of the drug or NP between tissue and blood. When the AUC is calculated based on the data in the unit of %ID, the distribution coefficient assesses the ratio of the total drug amount between the target tissue and the blood, whereas when the AUC is calculated based on the data in the unit of %ID/g, distribution coefficient can assess the ratio of the concentration between the target tissue and the blood.

In PK Parameter #2, the maximum concentration (C_{max}) was defined as the highest concentration in the unit of %ID or %ID/g tissue determined by visual inspection.

In PK Parameter #3, the AUC in blood was also calculated from 0 to t_{last} using the same method as PK Parameter #1. Thus, the distribution coefficient, which is expressed as the ratio of tumor AUC and blood AUC, was calculated with the following equation (Figure 2).

$$\text{Distribution Coefficient}_{\text{Tumor/Blood}} = \text{AUC}_{\text{tumor}}/\text{AUC}_{\text{blood}} \quad (4)$$

Notably, unlike PK Parameter #1 and Parameter #2, the third PK parameter of the distribution coefficient was calculated using ratios instead of percentages. Based on eq 4, the distribution coefficient is unitless. Hereinafter, the distribution coefficient (%ID) and distribution coefficient (%ID/g) represent the distribution coefficient that was derived using the concentration data in the units of %ID and %ID/g tissue, respectively.

Subgroup Statistical Analyses. To assess the impacts of physiological and physicochemical properties and other experimental factors, the tumor delivery, presented as tumor DE, tumor C_{max}, and tumor distribution coefficient, was summarized in various subgroups, including NP type, core material, shape, hydrodynamic size, PDI, zeta potential/surface charge, administrative dose, targeting strategy, tumor model, and the year of publication. For surface charge, the zeta potential ranges of less than −10 mV, −10 to 10 mV, and >10 mV were categorically defined as negative, neutral, and positive, respectively. Based on the hydrodynamic size, NPs were categorized into "<10 nm", "10−100 nm", "100−200 nm", and ">200 nm". The impact of administrative dose was also assessed using the magnitude group (i.e., "$<10^{-2}$", "10^{-2}", "10^{-1}", "10^{0}", "10^{1}", "10^{2}", "$>10^{2}$", and "Unknown"). A magnitude group, 10^{0}, for example, included an administrative dose ranging from 1 to 9.99 mg/kg.

To test whether there is a significant difference between different subgroups, one-way ANOVA (or Kruskal−Wallis test as appropriate) and simple linear regression were conducted to examine the significance of categorical and continuous variables, respectively. The medians of the tumor delivery efficiency data from the earlier version[9] of the "Nano-Tumor Database" based on data from 2005 to 2018 and the recently collected data were compared using a Mann−Whitney test. The variables with p-value < 0.05 were identified as statistically significant. Before testing, Shapiro-Wilk tests were conducted to test the normality of the PK parameter data with or without log-transformation. According to these results, the log-transformed data were (or more likely to be) normally distributed. Therefore, the data of these three PK parameters were log-transformed for further statistical analysis.

Before conducting the one-way ANOVA test, the assumption of equal variance was examined for log-transformed parameter data using Bartlett's test. A p-value of less than 0.05 indicates that the variance among subgroups was not significantly different. For the subgroup with a p-value less than 0.05, a Kruskal−Wallis test was performed, which was considered the nonparametric equivalent to a one-way ANOVA.[110] For the significant single categorical predictor derived from one-way ANOVA and Kruskal−Wallis test, pairwise comparisons were performed using a DSCF test.[145−147]

Multivariable linear regression was applied to investigate the impacts of the physicochemical characteristics on tumor delivery, including the core material, hydrodynamic size, zeta potential/surface charge, NP type, targeting strategy, cancer type, and tumor model. Multivariable linear regression was also conducted in some main subgroups, including ONMs, INMs, polymeric NPs, and gold NPs. To investigate the optimal NP design with a relatively higher tumor DE (PK Parameter #1), a simulation was performed for different combinations of NP features 1000 times. Representative simulated scenarios with the calculated percentage of injected dose of >3% or even >5% are presented for the group of all NPs and the subgroups of INMs, ONMs, and gold NPs, respectively.

To investigate the effects of the physicochemical parameters on the distribution of NPs in major healthy organs, multivariate analysis of variance (MANOVA) was applied to the NP type, core material,

https://doi.org/10.1021/acsnano.3c04037
ACS Nano 2023, 17, 19810−19831

targeting strategy, cancer type, tumor model, shape, size, and surface charge to test the effects of the physicochemical properties on the biodistribution difference among organs.

The calculation of PK parameters and all subgroup statistical analyses were conducted using R program (Version 4.2.2).[148]

ASSOCIATED CONTENT

Supporting Information

The Supporting Information is available free of charge at https://pubs.acs.org/doi/10.1021/acsnano.3c04037.

Word file that contains additional methods, additional results, Figures S1−S13, and Tables S1−S22 (PDF)

Excel file that contains the raw data of the updated "Nano-Tumor Database" (XLSX)

Zipped file that contains all R code files that were used to generate the results for each figure and table, as well as all the original results (ZIP)

AUTHOR INFORMATION

Corresponding Author

Zhoumeng Lin − *Department of Environmental and Global Health, College of Public Health and Health Professions, University of Florida, Gainesville, Florida 32608, United States; Center for Environmental and Human Toxicology, University of Florida, Gainesville, Florida 32610, United States;* orcid.org/0000-0002-8731-8366; Phone: + 1-352-273-6160; Email: linzhoumeng@ufl.edu

Authors

Qiran Chen − *Department of Environmental and Global Health, College of Public Health and Health Professions, University of Florida, Gainesville, Florida 32608, United States; Center for Environmental and Human Toxicology, University of Florida, Gainesville, Florida 32610, United States*

Long Yuan − *Department of Environmental and Global Health, College of Public Health and Health Professions, University of Florida, Gainesville, Florida 32608, United States; Center for Environmental and Human Toxicology, University of Florida, Gainesville, Florida 32610, United States*

Wei-Chun Chou − *Department of Environmental and Global Health, College of Public Health and Health Professions, University of Florida, Gainesville, Florida 32608, United States; Center for Environmental and Human Toxicology, University of Florida, Gainesville, Florida 32610, United States;* orcid.org/0000-0003-3355-6921

Yi-Hsien Cheng − *Department of Anatomy and Physiology, Kansas State University, Manhattan, Kansas 66506, United States; Institute of Computational Comparative Medicine, Kansas State University, Manhattan, Kansas 66506, United States;* orcid.org/0000-0002-4314-9732

Chunla He − *Department of Environmental and Global Health, College of Public Health and Health Professions, University of Florida, Gainesville, Florida 32608, United States; Department of Biostatistics College of Public Health and Health Professions, University of Florida, Gainesville, Florida 32608, United States*

Nancy A. Monteiro-Riviere − *Nanotechnology Innovation Center of Kansas State, Kansas State University, Manhattan, Kansas 66506, United States; Center for Chemical Toxicology Research and Pharmacokinetics, North Carolina State University, Raleigh, North Carolina 27606, United States;* orcid.org/0000-0002-0132-0861

Jim E. Riviere − *Center for Chemical Toxicology Research and Pharmacokinetics, North Carolina State University, Raleigh, North Carolina 27606, United States; 1 Data Consortium, Kansas State University, Olathe, Kansas 66061, United States*

Complete contact information is available at: https://pubs.acs.org/10.1021/acsnano.3c04037

Author Contributions

⊕These authors contributed equally to this work.

Funding

The study was supported by National Institute of Biomedical Imaging and Bioengineering of National Institutes of Health (Grant No. R01EB031022).

Notes

The authors declare no competing financial interest.

The Excel file and the zipped file are also available in GitHub (https://github.com/UFPBPK/Nano-Tumor-Database-Version2023).

REFERENCES

(1) Brigger, I.; Dubernet, C.; Couvreur, P. Nanoparticles in Cancer Therapy and Diagnosis. *Adv. Drug Delivery Rev.* **2012**, *64*, 24−36.

(2) Farjadian, F.; Ghasemi, A.; Gohari, O.; Roointan, A.; Karimi, M.; Hamblin, M. R. Nanopharmaceuticals and Nanomedicines Currently on the Market: Challenges and Opportunities. *Nanomedicine (Lond)* **2019**, *14*, 93−126.

(3) Gelperina, S.; Kisich, K.; Iseman, M. D.; Heifets, L. The Potential Advantages of Nanoparticle Drug Delivery Systems in Chemotherapy of Tuberculosis. *Am. J. Respir. Crit. Care Med.* **2005**, *172*, 1487−1490.

(4) Anselmo, A. C.; Mitragotri, S. Nanoparticles in the Clinic: An Update. *Bioeng. Transl. Med.* **2019**, *4*, No. e10143.

(5) Wilhelm, S.; Tavares, A. J.; Dai, Q.; Ohta, S.; Audet, J.; Dvorak, H. F.; Chan, W. C. W. Analysis of Nanoparticle Delivery to Tumours. *Nat. Rev. Mater.* **2016**, *1*, 16014.

(6) Metselaar, J. M.; Lammers, T. Challenges in Nanomedicine Clinical Translation. *Drug Delivery Transl. Res.* **2020**, *10*, 721−725.

(7) Chen, Q.; Riviere, J.; Lin, Z. Toxicokinetics, Dose-Response and Risk Assessment of Nanomaterials: Methodology, Challenges, and Future Perspectives. *WIREs Nanomed. Nanobiotechnol.* **2022**, *14*, No. e1808, DOI: 10.1002/wnan.1808.

(8) Overchuk, M.; Zheng, G. Overcoming Obstacles in the Tumor Microenvironment: Recent Advancements in Nanoparticle Delivery for Cancer Theranostics. *Biomaterials* **2018**, *156*, 217−237.

(9) Cheng, Y. H.; He, C.; Riviere, J. E.; Monteiro-Riviere, N. A.; Lin, Z. Meta-Analysis of Nanoparticle Delivery to Tumors Using a Physiologically Based Pharmacokinetic Modeling and Simulation Approach. *ACS Nano* **2020**, *14*, 3075−3095.

(10) Price, L. S. L.; Stern, S. T.; Deal, A. M.; Kabanov, A. V.; Zamboni, W. C. A Reanalysis of Nanoparticle Tumor Delivery Using Classical Pharmacokinetic Metrics. *Sci. Adv.* **2020**, *6*, No. eaay9249.

(11) Fan, F.; Xie, B.; Yang, L. Promoting Nanoparticle Delivery Efficiency to Tumors by Locally Increasing Blood Flow There. *ACS Appl. Bio. Mater.* **2021**, *4*, 7615−7625.

(12) Sun, B.; Luo, C.; Zhang, X.; Guo, M.; Sun, M.; Yu, H.; Chen, Q.; Yang, W.; Wang, M.; Zuo, S.; Chen, P.; Kan, Q.; Zhang, H.; Wang, Y.; He, Z.; Sun, J. Probing the Impact of Sulfur/Selenium/Carbon Linkages on Prodrug Nanoassemblies for Cancer Therapy. *Nat. Commun.* **2019**, *10*, 3211.

(13) Turan, O.; Bielecki, P.; Perera, V.; Lorkowski, M.; Covarrubias, G.; Tong, K.; Yun, A.; Rahmy, A.; Ouyang, T.; Raghunathan, S.; et al. Delivery of Drugs into Brain Tumors Using Multicomponent Silica Nanoparticles. *Nanoscale* **2019**, *11*, 11910−11921.

(14) Chen, J.; Yang, Q.; Liu, M.; Lin, M.; Wang, T.; Zhang, Z.; Zhong, X.; Guo, N.; Lu, Y.; Xu, J.; Wang, C.; Han, M.; Wei, Q. Remarkable Boron Delivery of Irgd-Modified Polymeric Nanoparticles for Boron Neutron Capture Therapy. *Int. J. Nanomedicine* **2019**, *14*, 8161−8177.
(15) Sun, C. Y.; Zhang, B. B.; Zhou, J. Y. Light-Activated Drug Release from a Hyaluronic Acid Targeted Nanoconjugate for Cancer Therapy. *J. Mater. Chem. B* **2019**, *7*, 4843−4853.
(16) Goos, J.; Cho, A.; Carter, L. M.; Dilling, T. R.; Davydova, M.; Mandleywala, K.; Puttick, S.; Gupta, A.; Price, W. S.; Quinn, J. F.; Whittaker, M. R.; Lewis, J. S.; Davis, T. P. Delivery of Polymeric Nanostars for Molecular Imaging and Endoradiotherapy through the Enhanced Permeability and Retention (Epr) Effect. *Theranostics* **2020**, *10*, 567−584.
(17) Liu, J.; Zhang, D.; Lian, S.; Zheng, J.; Li, B.; Li, T.; Jia, L. Redox-Responsive Hyaluronic Acid-Functionalized Graphene Oxide Nanosheets for Targeted Delivery of Water-Insoluble Cancer Drugs. *Int. J. Nanomedicine* **2018**, *13*, 7457−7472.
(18) Qian, X.; Ge, L.; Yuan, K.; Li, C.; Zhen, X.; Cai, W.; Cheng, R.; Jiang, X. Targeting and Microenvironment-Improving of Phenylboronic Acid-Decorated Soy Protein Nanoparticles with Different Sizes to Tumor. *Theranostics* **2019**, *9*, 7417−7430.
(19) Fan, C. H.; Wang, T. W.; Hsieh, Y. K.; Wang, C. F.; Gao, Z.; Kim, A.; Nagasaki, Y.; Yeh, C. K. Enhancing Boron Uptake in Brain Glioma by a Boron-Polymer/Microbubble Complex with Focused Ultrasound. *ACS Appl. Mater. Interfaces* **2019**, *11*, 11144−11156.
(20) Ren, L.; Feng, W.; Shao, J.; Ma, J.; Xu, M.; Zhu, B. Z.; Zheng, N.; Liu, S. Diethyldithiocarbamate-Copper Nanocomplex Reinforces Disulfiram Chemotherapeutic Efficacy through Light-Triggered Nuclear Targeting. *Theranostics* **2020**, *10*, 6384−6398.
(21) Detappe, A.; Mathieu, C.; Jin, C.; Agius, M. P.; Diringer, M. C.; Tran, V. L.; Pivot, X.; Lux, F.; Tillement, O.; Kufe, D.; Ghoroghchian, P. P. Anti-Muc1-C Antibody-Conjugated Nanoparticles Potentiate the Efficacy of Fractionated Radiation Therapy. *Int. J. Radiat Oncol Biol. Phys.* **2020**, *108*, 1380−1389.
(22) Jiang, W.; Han, X.; Zhang, T.; Xie, D.; Zhang, H.; Hu, Y. An Oxygen Self-Evolving, Multistage Delivery System for Deeply Located Hypoxic Tumor Treatment. *Adv. Healthc. Mater.* **2020**, *9*, 1901303.
(23) Tsai, M. F.; Lo, Y. L.; Huang, Y. C.; Yu, C. C.; Wu, Y. T.; Su, C. H.; Wang, L. F. Multi-Stimuli-Responsive Dox Released from Magnetosome for Tumor Synergistic Theranostics. *Int. J. Nanomedicine* **2020**, *15*, 8623−8639.
(24) Zhou, M.; Huang, H.; Wang, D.; Lu, H.; Chen, J.; Chai, Z.; Yao, S. Q.; Hu, Y. Light-Triggered Pegylation/Depegylation of the Nanocarriers for Enhanced Tumor Penetration. *Nano Lett.* **2019**, *19*, 3671−3675.
(25) Li, X.; Zou, Q.; Zhang, J.; Zhang, P.; Zhou, X.; Yalamarty, S. S. K.; Liang, X.; Liu, Y.; Zheng, Q.; Gao, J. Self-Assembled Dual-Targeted Epirubicin-Hybrid Polydopamine Nanoparticles for Combined Chemo-Photothermal Therapy of Triple-Negative Breast Cancer. *Int. J. Nanomedicine* **2020**, *15*, 6791−6811.
(26) Tang, J.; Zeng, Z.; Yan, J.; Chen, C.; Liu, J.; Feng, X. Quantitative and High Drug Loading of Self-Assembled Prodrug with Defined Molecular Structures for Effective Cancer Therapy. *J. Controlled Release* **2019**, *307*, 90−97.
(27) Fu, C.; Duan, X.; Cao, M.; Jiang, S.; Ban, X.; Guo, N.; Zhang, F.; Mao, J.; Huyan, T.; Shen, J.; Zhang, L. M. Targeted Magnetic Resonance Imaging and Modulation of Hypoxia with Multifunctional Hyaluronic Acid-Mno_2 Nanoparticles in Glioma. *Adv. Healthc. Mater.* **2019**, *8*, 1900047.
(28) Wu, Q.; Chen, X.; Wang, P.; Wu, Q.; Qi, X.; Han, X.; Chen, L.; Meng, X.; Xu, K. Delivery of Arsenic Trioxide by Multifunction Nanoparticles to Improve the Treatment of Hepatocellular Carcinoma. *ACS Appl. Mater. Interfaces* **2020**, *12*, 8016−8029.
(29) Wang, H.; Zheng, M.; Gao, J.; Wang, J.; Zhang, Q.; Fawcett, J. P.; He, Y.; Gu, J. Uptake and Release Profiles of Pegylated Liposomal Doxorubicin Nanoparticles: A Comprehensive Picture Based on Separate Determination of Encapsulated and Total Drug Concentrations in Tissues of Tumor-Bearing Mice. *Talanta* **2020**, *208*, 120358.
(30) Xu, Y.; Ren, H.; Liu, J.; Wang, Y.; Meng, Z.; He, Z.; Miao, W.; Chen, G.; Li, X. A Switchable No-Releasing Nanomedicine for Enhanced Cancer Therapy and Inhibition of Metastasis. *Nanoscale* **2019**, *11*, 5474−5488.
(31) Stras, S.; Howe, A.; Prasad, A.; Salerno, D.; Bhatavdekar, O.; Sofou, S. Growth of Metastatic Triple-Negative Breast Cancer Is Inhibited by Deep Tumor-Penetrating and Slow Tumor-Clearing Chemotherapy: The Case of Tumor-Adhering Liposomes with Interstitial Drug Release. *Mol. Pharmaceutics* **2020**, *17*, 118−131.
(32) Zhang, D.; Qin, X.; Wu, T.; Qiao, Q.; Song, Q.; Zhang, Z. Extracellular Vesicles Based Self-Grown Gold Nanopopcorn for Combinatorial Chemo-Photothermal Therapy. *Biomaterials* **2019**, *197*, 220−228.
(33) Goel, S.; Ferreira, C. A.; Dogra, P.; Yu, B.; Kutyreff, C. J.; Siamof, C. M.; Engle, J. W.; Barnhart, T. E.; Cristini, V.; Wang, Z.; Cai, W. Size-Optimized Ultrasmall Porous Silica Nanoparticles Depict Vasculature-Based Differential Targeting in Triple Negative Breast Cancer. *Small* **2019**, *15*, No. e1903747.
(34) Yang, R.; Hou, M.; Gao, Y.; Lu, S.; Zhang, L.; Xu, Z.; Li, C. M.; Kang, Y.; Xue, P. Biomineralization-Inspired Crystallization of Manganese Oxide on Silk Fibroin Nanoparticles for in Vivo Mr/Fluorescence Imaging-Assisted Tri-Modal Therapy of Cancer. *Theranostics* **2019**, *9*, 6314−6333.
(35) Wang, S.; Zhou, Z.; Wang, Z.; Liu, Y.; Jacobson, O.; Shen, Z.; Fu, X.; Chen, Z. Y.; Chen, X. Gadolinium Metallofullerene-Based Activatable Contrast Agent for Tumor Signal Amplification and Monitoring of Drug Release. *Small* **2019**, *15*, No. e1900691.
(36) Wang, Z.; Kuang, G.; Yu, Z.; Li, A.; Zhou, D.; Huang, Y. Light-Activatable Dual Prodrug Polymer Nanoparticle for Precise Synergistic Chemotherapy Guided by Drug-Mediated Computed Tomography Imaging. *Acta Biomater* **2019**, *94*, 459−468.
(37) Karimi, M.; Gheybi, F.; Zamani, P.; Mashreghi, M.; Golmohammadzadeh, S.; Darban, S. A.; Badiee, A.; Jaafari, M. R. Preparation and Characterization of Stable Nanoliposomal Formulations of Curcumin with High Loading Efficacy: In Vitro and in Vivo Anti-Tumor Study. *Int. J. Pharm.* **2020**, *580*, 119211.
(38) Sun, H.; Guo, X.; Zeng, S.; Wang, Y.; Hou, J.; Yang, D.; Zhou, S. A Multifunctional Liposomal Nanoplatform Co-Delivering Hydrophobic and Hydrophilic Doxorubicin for Complete Eradication of Xenografted Tumors. *Nanoscale* **2019**, *11*, 17759−17772.
(39) Sarparanta, M.; Pourat, J.; Carnazza, K. E.; Tang, J.; Paknejad, N.; Reiner, T.; Kostiainen, M. A.; Lewis, J. S. Multimodality Labeling Strategies for the Investigation of Nanocrystalline Cellulose Biodistribution in a Mouse Model of Breast Cancer. *Nucl. Med. Biol.* **2020**, *80*−*81*, 1−12.
(40) Kateh Shamshiri, M.; Jaafari, M. R.; Badiee, A. Preparation of Liposomes Containing Ifn-Gamma and Their Potentials in Cancer Immunotherapy: In Vitro and in Vivo Studies in a Colon Cancer Mouse Model. *Life Sci.* **2021**, *264*, 118605.
(41) Bai, L.; Yi, W.; Sun, T.; Tian, Y.; Zhang, P.; Si, J.; Hou, X.; Hou, J. Surface Modification Engineering of Two-Dimensional Titanium Carbide for Efficient Synergistic Multitherapy of Breast Cancer. *J. Mater. Chem. B* **2020**, *8*, 6402−6417.
(42) Darwish, W. M. A.; Bayoumi, N. A. Gold Nanorod-Loaded (Plga-Peg) Nanocapsules as near-Infrared Controlled Release Model of Anticancer Therapeutics. *Lasers Med. Sci.* **2020**, *35*, 1729−1740.
(43) Liu, Y.; Lang, T.; Zheng, Z.; Cheng, H.; Huang, X.; Wang, G.; Yin, Q.; Li, Y. In Vivo Environment-Adaptive Nanocomplex with Tumor Cell-Specific Cytotoxicity Enhances T Cells Infiltration and Improves Cancer Therapy. *Small* **2019**, *15*, No. e1902822.
(44) Cheng, Y.; Lu, T.; Wang, Y.; Song, Y.; Wang, S.; Lu, Q.; Yang, L.; Tan, F.; Li, J.; Li, N. Glutathione-Mediated Clearable Nanoparticles Based on Ultrasmall Gd_2o_3 for Msot/Ct/Mr Imaging Guided Photothermal/Radio Combination Cancer Therapy. *Mol. Pharmaceutics* **2019**, *16*, 3489−3501.
(45) Wang, R.; Yang, M.; Li, G.; Wang, X.; Zhang, Z.; Qiao, H.; Chen, J.; Chen, Z.; Cui, X.; Li, J. Paclitaxel-Betulinic Acid Hybrid

https://doi.org/10.1021/acsnano.3c04037
ACS Nano 2023, 17, 19810−19831

Nanosuspensions for Enhanced Anti-Breast Cancer Activity. *Colloids Surf., B* **2019**, *174*, 270−279.
(46) Yang, J.; Dai, D.; Lou, X.; Ma, L.; Wang, B.; Yang, Y. W. Supramolecular Nanomaterials Based on Hollow Mesoporous Drug Carriers and Macrocycle-Capped Cus Nanogates for Synergistic Chemo-Photothermal Therapy. *Theranostics* **2020**, *10*, 615−629.
(47) Wang, X.; Xu, J.; Xu, X.; Fang, Q.; Tang, R. Ph-Sensitive Bromelain Nanoparticles by Ortho Ester Crosslinkage for Enhanced Doxorubicin Penetration in Solid Tumor. *Mater. Sci. Eng. C Mater. Biol. Appl.* **2020**, *113*, 111004.
(48) Zeng, K.; Xu, Q.; Ouyang, J.; Han, Y.; Sheng, J.; Wen, M.; Chen, W.; Liu, Y. N. Coordination Nanosheets of Phthalocyanine as Multifunctional Platform for Imaging-Guided Synergistic Therapy of Cancer. *ACS Appl. Mater. Interfaces* **2019**, *11*, 6840−6849.
(49) Sakr, T. M.; Khowessah, O. M.; Motaleb, M. A.; Abd El-Bary, A.; El-Kolaly, M. T.; Swidan, M. M. I-131 Doping of Silver Nanoparticles Platform for Tumor Theranosis Guided Drug Delivery. *Eur. J. Pharm. Sci.* **2018**, *122*, 239−245.
(50) Liu, J.; Zheng, J.; Nie, H.; Zhang, D.; Cao, D.; Xing, Z.; Li, B.; Jia, L. Molybdenum Disulfide-Based Hyaluronic Acid-Guided Multi-functional Theranostic Nanoplatform for Magnetic Resonance Imaging and Synergetic Chemo-Photothermal Therapy. *J. Colloid Interface Sci.* **2019**, *548*, 131−144.
(51) Wang, Y.; Song, S.; Lu, T.; Cheng, Y.; Song, Y.; Wang, S.; Tan, F.; Li, J.; Li, N. Oxygen-Supplementing Mesoporous Polydopamine Nanosponges with Ws_2 Qds-Embedded for Ct/Msot/Mr Imaging and Thermoradiotherapy of Hypoxic Cancer. *Biomaterials* **2019**, *220*, 119405.
(52) Imlimthan, S.; Otaru, S.; Keinanen, O.; Correia, A.; Lintinen, K.; Santos, H. A.; Airaksinen, A. J.; Kostiainen, M. A.; Sarparanta, M. Radiolabeled Molecular Imaging Probes for the in Vivo Evaluation of Cellulose Nanocrystals for Biomedical Applications. *Biomacromolecules* **2019**, *20*, 674−683.
(53) Zhu, Y. H.; Wang, J. L.; Zhang, H. B.; Khan, M. I.; Du, X. J.; Wang, J. Incorporation of a Rhodamine B Conjugated Polymer for Nanoparticle Trafficking Both in Vitro and in Vivo. *Biomater. Sci.* **2019**, *7*, 1933−1939.
(54) Hao, X.; Xu, B.; Chen, H.; Wang, X.; Zhang, J.; Guo, R.; Shi, X.; Cao, X. Stem Cell-Mediated Delivery of Nanogels Loaded with Ultrasmall Iron Oxide Nanoparticles for Enhanced Tumor Mr Imaging. *Nanoscale* **2019**, *11*, 4904−4910.
(55) Mukai, H.; Hatanaka, K.; Yagi, N.; Warashina, S.; Zouda, M.; Takahashi, M.; Narushima, K.; Yabuuchi, H.; Iwano, J.; Kuboyama, T.; Enokizono, J.; Wada, Y.; Watanabe, Y. Pharmacokinetic Evaluation of Liposomal Nanoparticle-Encapsulated Nucleic Acid Drug: A Combined Study of Dynamic Pet Imaging and Lc/Ms/Ms Analysis. *J. Controlled Release* **2019**, *294*, 185−194.
(56) Liu, J.; Xu, F.; Huang, J.; Xu, J.; Liu, Y.; Yao, Y.; Ao, M.; Li, A.; Hao, L.; Cao, Y.; Hu, Z.; Ran, H.; Wang, Z.; Li, P. Low-Intensity Focused Ultrasound (Lifu)-Activated Nanodroplets as a Theranostic Agent for Noninvasive Cancer Molecular Imaging and Drug Delivery. *Biomater. Sci.* **2018**, *6*, 2838−2849.
(57) Li, Q.; Sun, L.; Hou, M.; Chen, Q.; Yang, R.; Zhang, L.; Xu, Z.; Kang, Y.; Xue, P. Phase-Change Material Packaged within Hollow Copper Sulfide Nanoparticles Carrying Doxorubicin and Chlorin E6 for Fluorescence-Guided Trimodal Therapy of Cancer. *ACS Appl. Mater. Interfaces* **2019**, *11*, 417−429.
(58) Wang, J. L.; Du, X. J.; Yang, J. X.; Shen, S.; Li, H. J.; Luo, Y. L.; Iqbal, S.; Xu, C. F.; Ye, X. D.; Cao, J.; Wang, J. The Effect of Surface Poly(Ethylene Glycol) Length on in Vivo Drug Delivery Behaviors of Polymeric Nanoparticles. *Biomaterials* **2018**, *182*, 104−113.
(59) Liu, M.; Li, C.; Na Yan; Zhao, D.; Zhang, H.; Li, J.; Tang, X.; Liu, X.; Deng, Y.; Song, Y. Influence of Dose on Neutrophil-Mediated Delivery of Nanoparticles for Tumor-Targeting Therapy Strategies. *AAPS PharmSciTech* **2021**, *22*, 89.
(60) Park, J. E.; Park, J.; Jun, Y.; Oh, Y.; Ryoo, G.; Jeong, Y. S.; Gadalla, H. H.; Min, J. S.; Jo, J. H.; Song, M. G.; Kang, K. W.; Bae, S. K.; Yeo, Y.; Lee, W. Expanding Therapeutic Utility of Carfilzomib for Breast Cancer Therapy by Novel Albumin-Coated Nanocrystal Formulation. *J. Controlled Release* **2019**, *302*, 148−159.
(61) Yu, G.; Yu, S.; Saha, M. L.; Zhou, J.; Cook, T. R.; Yung, B. C.; Chen, J.; Mao, Z.; Zhang, F.; Zhou, Z.; Liu, Y.; Shao, L.; Wang, S.; Gao, C.; Huang, F.; Stang, P. J.; Chen, X. A Discrete Organoplatinum-(Ii) Metallacage as a Multimodality Theranostic Platform for Cancer Photochemotherapy. *Nat. Commun.* **2018**, *9*, 4335.
(62) Jin, Z.; Li, J. S.; Tang, D. N. Potential of Utilization of Albumin as a Delivery Module in Cancer Model. *J. BUON* **2019**, *24*, 347−353.
(63) He, L.; Qing, F.; Li, M.; Lan, D. Paclitaxel/Ir1061-Co-Loaded Protein Nanoparticle for Tumor-Targeted and Ph/Nir-Ii-Triggered Synergistic Photothermal-Chemotherapy. *Int. J. Nanomedicine* **2020**, *15*, 2337−2349.
(64) Qiu, R.; Qian, F.; Wang, X.; Li, H.; Wang, L. Targeted Delivery of 20(S)-Ginsenoside Rg3-Based Polypeptide Nanoparticles to Treat Colon Cancer. *Biomed. Microdevices* **2019**, *21*, 18.
(65) Zhang, J.; Shen, L.; Li, X.; Song, W.; Liu, Y.; Huang, L. Nanoformulated Codelivery of Quercetin and Alantolactone Promotes an Antitumor Response through Synergistic Immunogenic Cell Death for Microsatellite-Stable Colorectal Cancer. *ACS Nano* **2019**, *13*, 12511−12524.
(66) Parashar, P.; Tripathi, C. B.; Arya, M.; Kanoujia, J.; Singh, M.; Yadav, A.; Kaithwas, G.; Saraf, S. A. A Synergistic Approach for Management of Lung Carcinoma through Folic Acid Functionalized Co-Therapy of Capsaicin and Gefitinib Nanoparticles: Enhanced Apoptosis and Metalloproteinase-9 Down-Regulation. *Phytomedicine* **2019**, *53*, 107−123.
(67) Yu, G.; Zhu, B.; Shao, L.; Zhou, J.; Saha, M. L.; Shi, B.; Zhang, Z.; Hong, T.; Li, S.; Chen, X.; Stang, P. J. Host-Guest Complexation-Mediated Codelivery of Anticancer Drug and Photosensitizer for Cancer Photochemotherapy. *Proc. Natl. Acad. Sci. U. S. A.* **2019**, *116*, 6618−6623.
(68) Feng, J.; Yu, W.; Xu, Z.; Hu, J.; Liu, J.; Wang, F. Multifunctional Sirna-Laden Hybrid Nanoplatform for Noninvasive Pa/Ir Dual-Modal Imaging-Guided Enhanced Photogenetherapy. *ACS Appl. Mater. Interfaces* **2020**, *12*, 22613−22623.
(69) Zhang, H. J.; Zhao, X.; Chen, L. J.; Yang, C. X.; Yan, X. P. Ph-Driven Targeting Nanoprobe with Dual-Responsive Drug Release for Persistent Luminescence Imaging and Chemotherapy of Tumor. *Anal. Chem.* **2020**, *92*, 1179−1188.
(70) Shi, X.; Shen, L. Integrin $A_v\beta_3$ Receptor Targeting Pet/Mri Dual-Modal Imaging Probe Based on the ^{64}cu Labeled Manganese Ferrite Nanoparticles. *J. Inorg. Biochem.* **2018**, *186*, 257−263.
(71) Liu, J.; Li, F.; Zheng, J.; Li, B.; Zhang, D.; Jia, L. Redox/NIR Dual-Responsive Mos2 for Synergetic Chemo-Photothermal Therapy of Cancer. *J. Nanobiotechnology* **2019**, *17*, 78.
(72) Chen, F.; Ma, K.; Madajewski, B.; Zhuang, L.; Zhang, L.; Rickert, K.; Marelli, M.; Yoo, B.; Turker, M. Z.; Overholtzer, M.; Quinn, T. P.; Gonen, M.; Zanzonico, P.; Tuesca, A.; Bowen, M. A.; Norton, L.; Subramony, J. A.; Wiesner, U.; Bradbury, M. S. Ultrasmall Targeted Nanoparticles with Engineered Antibody Fragments for Imaging Detection of Her2-Overexpressing Breast Cancer. *Nat. Commun.* **2018**, *9*, 4141.
(73) Wang, Y.; Zhang, Y.; Ru, Z.; Song, W.; Chen, L.; Ma, H.; Sun, L. A ROS-Responsive Polymeric Prodrug Nanosystem with Self-Amplified Drug Release for Psma (−) Prostate Cancer Specific Therapy. *J. Nanobiotechnology* **2019**, *17*, 91.
(74) Bao, Y. W.; Hua, X. W.; Chen, X.; Wu, F. G. Platinum-Doped Carbon Nanoparticles Inhibit Cancer Cell Migration under Mild Laser Irradiation: Multi-Organelle-Targeted Photothermal Therapy. *Biomaterials* **2018**, *183*, 30−42.
(75) Ren, L.; Liu, X.; Ji, T.; Deng, G.; Liu, F.; Yuan, H.; Yu, J.; Hu, J.; Lu, J. All-in-One″ Theranostic Agent with Seven Functions Based on Bi-Doped Metal Chalcogenide Nanoflowers. *ACS Appl. Mater. Interfaces* **2019**, *11*, 45467−45478.
(76) Rainone, P.; De Palma, A.; Sudati, F.; Roffia, V.; Rigamonti, V.; Salvioni, L.; Colombo, M.; Ripamonti, M.; Spinelli, A. E.; Mazza, D.; Mauri, P.; Moresco, R. M.; Prosperi, D.; Belloli, S. ^{99m}tc-Radiolabeled

Silica Nanocarriers for Targeted Detection and Treatment of Her2-Positive Breast Cancer. *Int. J. Nanomedicine* **2021**, *16*, 1943−1960.
(77) Fan, W.; Lu, N.; Shen, Z.; Tang, W.; Shen, B.; Cui, Z.; Shan, L.; Yang, Z.; Wang, Z.; Jacobson, O.; Zhou, Z.; Liu, Y.; Hu, P.; Yang, W.; Song, J.; Zhang, Y.; Zhang, L.; Khashab, N. M.; Aronova, M. A.; Lu, G.; Chen, X. Generic Synthesis of Small-Sized Hollow Mesoporous Organosilica Nanoparticles for Oxygen-Independent X-Ray-Activated Synergistic Therapy. *Nat. Commun.* **2019**, *10*, 1241.
(78) Zhang, D. Y.; Zheng, Y.; Zhang, H.; Yang, G. G.; Tan, C. P.; He, L.; Ji, L. N.; Mao, Z. W. Folate Receptor-Targeted Theranostic Irsx Nanoparticles for Multimodal Imaging-Guided Combined Chemo-Photothermal Therapy. *Nanoscale* **2018**, *10*, 22252−22262.
(79) He, Y.; Shao, L.; Usman, I.; Hu, Y.; Pan, A.; Liang, S.; Xu, H. A Ph-Responsive Dissociable Mesoporous Silica-Based Nanoplatform Enabling Efficient Dual-Drug Co-Delivery and Rapid Clearance for Cancer Therapy. *Biomater. Sci.* **2020**, *8*, 3418−3429.
(80) Theune, L. E.; Buchmann, J.; Wedepohl, S.; Molina, M.; Laufer, J.; Calderon, M. Nir- and Thermo-Responsive Semi-Interpenetrated Polypyrrole Nanogels for Imaging Guided Combinational Photothermal and Chemotherapy. *J. Controlled Release* **2019**, *311*−*312*, 147−161.
(81) Ding, Y.; Du, C.; Qian, J.; Dong, C. M. Nir-Responsive Polypeptide Nanocomposite Generates No Gas, Mild Photothermia, and Chemotherapy to Reverse Multidrug-Resistant Cancer. *Nano Lett.* **2019**, *19*, 4362−4370.
(82) Lang, T.; Liu, Y.; Zheng, Z.; Ran, W.; Zhai, Y.; Yin, Q.; Zhang, P.; Li, Y. Cocktail Strategy Based on Spatio-Temporally Controlled Nano Device Improves Therapy of Breast Cancer. *Adv. Mater.* **2019**, *31*, No. e1903844.
(83) Xie, S.; Chen, M.; Song, X.; Zhang, Z.; Zhang, Z.; Chen, Z.; Li, X. Bacterial Microbots for Acid-Labile Release of Hybrid Micelles to Promote the Synergistic Antitumor Efficacy. *Acta Biomater* **2018**, *78*, 198−210.
(84) Wang, X.; Luo, J.; He, L.; Cheng, X.; Yan, G.; Wang, J.; Tang, R. Hybrid Ph-Sensitive Nanogels Surface-Functionalized with Collagenase for Enhanced Tumor Penetration. *J. Colloid Interface Sci.* **2018**, *525*, 269−281.
(85) Ma, B. A.; Sun, C. Y. Tumor Ph-Triggered "Charge Conversion" Nanocarriers with on-Demand Drug Release for Precise Cancer Therapy. *J. Mater. Chem. B* **2020**, *8*, 9351−9361.
(86) Garcia Ribeiro, R. S.; Belderbos, S.; Danhier, P.; Gallo, J.; Manshian, B. B.; Gallez, B.; Banobre, M.; de Cuyper, M.; Soenen, S. J.; Gsell, W.; Himmelreich, U. Targeting Tumor Cells and Neovascularization Using Rgd-Functionalized Magnetoliposomes. *Int. J. Nanomedicine* **2019**, *14*, 5911−5924.
(87) Wu, J.; Niu, S.; Bremner, D. H.; Nie, W.; Fu, Z.; Li, D.; Zhu, L. M. A Tumor Microenvironment-Responsive Biodegradable Mesoporous Nanosystem for Anti-Inflammation and Cancer Theranostics. *Adv. Healthc. Mater.* **2020**, *9*, No. e1901307.
(88) Karges, J.; Li, J.; Zeng, L.; Chao, H.; Gasser, G. Polymeric Encapsulation of a Ruthenium Polypyridine Complex for Tumor Targeted One- and Two-Photon Photodynamic Therapy. *ACS Appl. Mater. Interfaces* **2020**, *12*, 54433−54444.
(89) Zhang, H.; Zhu, Y.; Sun, C.; Xie, Y.; Adu-Frimpong, M.; Deng, W.; Yu, J.; Xu, X.; Han, Z.; Qi, G. Gsh Responsive Nanomedicines Self-Assembled from Small Molecule Prodrug Alleviate the Toxicity of Cardiac Glycosides as Potent Cancer Drugs. *Int. J. Pharm.* **2020**, *575*, 118980.
(90) Lin, Q.; Qu, M.; Zhou, B.; Patra, H. K.; Sun, Z.; Luo, Q.; Yang, W.; Wu, Y.; Zhang, Y.; Li, L.; Deng, L.; Wang, L.; Gong, T.; He, Q.; Zhang, L.; Sun, X.; Zhang, Z. Exosome-Like Nanoplatform Modified with Targeting Ligand Improves Anti-Cancer and Anti-Inflammation Effects of Imperialine. *J. Controlled Release* **2019**, *311*−*312*, 104−116.
(91) Xie, Z.; Liang, S.; Cai, X.; Ding, B.; Huang, S.; Hou, Z.; Ma, P.; Cheng, Z.; Lin, J. O_2-Cu/Zif-8@Ce6/Zif-8@F127 Composite as a Tumor Microenvironment-Responsive Nanoplatform with Enhanced Photo-/Chemodynamic Antitumor Efficacy. *ACS Appl. Mater. Interfaces* **2019**, *11*, 31671−31680.
(92) Faruqu, F. N.; Wang, J. T.; Xu, L.; McNickle, L.; Chong, E. M.; Walters, A.; Gurney, M.; Clayton, A.; Smyth, L. A.; Hider, R.; Sosabowski, J.; Al-Jamal, K. T. Membrane Radiolabelling of Exosomes for Comparative Biodistribution Analysis in Immunocompetent and Immunodeficient Mice - a Novel and Universal Approach. *Theranostics* **2019**, *9*, 1666−1682.
(93) Ming, J.; Zhang, J.; Shi, Y.; Yang, W.; Li, J.; Sun, D.; Xiang, S.; Chen, X.; Chen, L.; Zheng, N. A Trustworthy Cpg Nanoplatform for Highly Safe and Efficient Cancer Photothermal Combined Immunotherapy. *Nanoscale* **2020**, *12*, 3916−3930.
(94) Cherukula, K.; Uthaman, S.; Park, I. K. Navigate-Dock-Activate" Anti-Tumor Strategy: Tumor Micromilieu Charge-Switchable, Hierarchically Activated Nanoplatform with Ultrarapid Tumor-Tropic Accumulation for Trackable Photothermal/Chemotherapy. *Theranostics* **2019**, *9*, 2505−2525.
(95) Wei, R.; Gong, X.; Lin, H.; Zhang, K.; Li, A.; Liu, K.; Shan, H.; Chen, X.; Gao, J. Versatile Octapod-Shaped Hollow Porous Manganese(Ii) Oxide Nanoplatform for Real-Time Visualization of Cargo Delivery. *Nano Lett.* **2019**, *19*, 5394−5402.
(96) Yang, G. G.; Zhang, H.; Zhang, D. Y.; Cao, Q.; Yang, J.; Ji, L. N.; Mao, Z. W. Cancer-Specific Chemotherapeutic Strategy Based on the Vitamin K3Mediated Ros Regenerative Feedback and Visualized Drug Release in Vivo. *Biomaterials* **2018**, *185*, 73−85.
(97) Sobol, N. B.; Korsen, J. A.; Younes, A.; Edwards, K. J.; Lewis, J. S. Immunopet Imaging of Pancreatic Tumors with ^{89}zr-Labeled Gold Nanoparticle-Antibody Conjugates. *Mol. Imaging Biol.* **2021**, *23*, 84−94.
(98) Long, Q.; Zhu, W.; Guo, L.; Pu, L. Rgd-Conjugated Resveratrol Hsa Nanoparticles as a Novel Delivery System in Ovarian Cancer Therapy. *Drug Des. Devel. Ther.* **2020**, *14*, 5747−5756.
(99) El-Safoury, D. M.; Ibrahim, A. B.; El-Setouhy, D. A.; Khowessah, O. M.; Motaleb, M. A.; Sakr, T. M. Amelioration of Tumor Targeting and in Vivo Biodistribution of ^{99m}tc-Methotrexate-Gold Nanoparticles (^{99m}tc-Mex-Aunps). *J. Pharm. Sci.* **2021**, *110*, 2955−2965.
(100) Qian, X.; Shen, T.; Zhang, X.; Wang, C.; Cai, W.; Cheng, R.; Jiang, X. Biologically Active Camellia Oleifera Protein Nanoparticles for Improving the Tumor Microenvironment and Drug Delivery. *Biomater. Sci.* **2020**, *8*, 3907−3915.
(101) Huang, J. R.; Lee, M. H.; Li, W. S.; Wu, H. C. Liposomal Irinotecan for Treatment of Colorectal Cancer in a Preclinical Model. *Cancers (Basel)* **2019**, *11*, 281.
(102) Xu, Y.; Tang, L.; Liu, Y.; Qian, C.; Chen, P.; Xin, Y.; Liu, H.; Qu, Y. Dual-Modified Albumin-Polymer Nanocomplexes with Enhanced in Vivo Stability for Hepatocellular Carcinoma Therapy. *Colloids Surf., B* **2021**, *201*, 111642.
(103) Xu, L.; Wang, Y.; Zhu, C.; Ren, S.; Shao, Y.; Wu, L.; Li, W.; Jia, X.; Hu, R.; Chen, R.; Chen, Z. Morphological Transformation Enhances Tumor Retention by Regulating the Self-Assembly of Doxorubicin-Peptide Conjugates. *Theranostics* **2020**, *10*, 8162−8178.
(104) Mu, J.; Zhong, H.; Zou, H.; Liu, T.; Yu, N.; Zhang, X.; Xu, Z.; Chen, Z.; Guo, S. Acid-Sensitive Pegylated Paclitaxel Prodrug Nanoparticles for Cancer Therapy: Effect of Peg Length on Antitumor Efficacy. *J. Controlled Release* **2020**, *326*, 265−275.
(105) Zhou, L.; Chen, L.; Hu, X.; Lu, Y.; Liu, W.; Sun, Y.; Yao, T.; Dong, C.; Shi, S. A Cu_9s_5 Nanoparticle-Based Cpg Delivery System for Synergistic Photothermal-, Photodynamic- and Immunotherapy. *Commun. Biol.* **2020**, *3*, 343.
(106) Zhong, P.; Chen, X.; Guo, R.; Chen, X.; Chen, Z.; Wei, C.; Li, Y.; Wang, W.; Zhou, Y.; Qin, L. Folic Acid-Modified Nanoerythrocyte for Codelivery of Paclitaxel and Tariquidar to Overcome Breast Cancer Multidrug Resistance. *Mol. Pharmaceutics* **2020**, *17*, 1114−1126.
(107) Sousa-Junior, A. A.; Mendanha, S. A.; Carriao, M. S.; Capistrano, G.; Prospero, A. G.; Soares, G. A.; Cintra, E. R.; Santos, S. F. O.; Zufelato, N.; Alonso, A.; Lima, E. M.; Miranda, J. R. A.; Silveira-Lacerda, E. P.; Cardoso, C. G.; Bakuzis, A. F. Predictive Model for Delivery Efficiency: Erythrocyte Membrane-Camouflaged

https://doi.org/10.1021/acsnano.3c04037
ACS Nano 2023, 17, 19810−19831

Magnetofluorescent Nanocarriers Study. *Mol. Pharmaceutics* **2020**, *17*, 837−851.
(108) Kunii, R.; Onishi, H.; Ueki, K.; Koyama, K.; Machida, Y. Particle Characteristics and Biodistribution of Camptothecin-Loaded Pla/(Peg-Ppg-Peg) Nanoparticles. *Drug Delivery* **2008**, *15*, 3−10.
(109) Chan, W. Principles of Nanoparticle Delivery to Solid Tumours. *BMEF (BME Frontiers) Article* **2023**, *4*, 0016.
(110) Dalgaard, P. Analysis of Variance and the Kruskal-Wallis Test. *Introductory Statistics with R* **2008**, 127−143.
(111) Lin, Z.; Monteiro-Riviere, N. A.; Riviere, J. E. Pharmacokinetics of Metallic Nanoparticles. *Wiley Interdiscip. Rev.: Nanomed. Nanobiotechnol.* **2015**, *7*, 189−217.
(112) Bromma, K.; Chithrani, D. B. Advances in Gold Nanoparticle-Based Combined Cancer Therapy. *Nanomaterials (Basel)* **2020**, *10*, 1671.
(113) Lin, Z.; Aryal, S.; Cheng, Y.; Gesquiere, A. Integration of in Vitro and in Vivo Models to Predict Cellular and Tissue Dosimetry of Nanomaterials Using Physiologically Based Pharmacokinetic Modeling. *ACS Nano* **2022**, *16*, 19722−19754.
(114) Large, D. E.; Abdelmessih, R. G.; Fink, E. A.; Auguste, D. T. Liposome Composition in Drug Delivery Design, Synthesis, Characterization, and Clinical Application. *Adv. Drug Deliv Rev.* **2021**, *176*, 113851.
(115) Talens-Visconti, R.; Diez-Sales, O.; de Julian-Ortiz, J. V.; Nacher, A. Nanoliposomes in Cancer Therapy: Marketed Products and Current Clinical Trials. *Int. J. Mol. Sci.* **2022**, *23*, 4249.
(116) Wang, J.; Byrne, J. D.; Napier, M. E.; DeSimone, J. M. More Effective Nanomedicines through Particle Design. *Small* **2011**, *7*, 1919−1931.
(117) Wang, H. X.; Zuo, Z. Q.; Du, J. Z.; Wang, Y. C.; Sun, R.; Cao, Z. T.; Ye, X. D.; Wang, J. L.; Leong, K. W.; Wang, J. Surface Charge Critically Affects Tumor Penetration and Therapeutic Efficacy of Cancer Nanomedicines. *Nano Today* **2016**, *11*, 133−144.
(118) Zhang, Y. R.; Lin, R.; Li, H. J.; He, W. l.; Du, J. Z.; Wang, J. Strategies to Improve Tumor Penetration of Nanomedicines through Nanoparticle Design. *Wiley Interdiscip. Rev.: Nanomed. Nanobiotechnol.* **2019**, *11*, No. e1519.
(119) Jain, R. K.; Stylianopoulos, T. Delivering Nanomedicine to Solid Tumors. *Nat. Rev. Clin. Oncol.* **2010**, *7*, 653−664.
(120) Ouyang, B.; Poon, W.; Zhang, Y. N.; Lin, Z. P.; Kingston, B. R.; Tavares, A. J.; Zhang, Y.; Chen, J.; Valic, M. S.; Syed, A. M.; MacMillan, P.; Couture-Senecal, J.; Zheng, G.; Chan, W. C. W. The Dose Threshold for Nanoparticle Tumour Delivery. *Nat. Mater.* **2020**, *19*, 1362−1371.
(121) Zhong, J.; Wen, L.; Yang, S.; Xiang, L.; Chen, Q.; Xing, D. Imaging-Guided High-Efficient Photoacoustic Tumor Therapy with Targeting Gold Nanorods. *Nanomedicine* **2015**, *11*, 1499−509.
(122) Wu, T.; Tang, M. Review of the Effects of Manufactured Nanoparticles on Mammalian Target Organs. *J. Appl. Toxicol.* **2018**, *38*, 25−40.
(123) An, S. S. A.; Lee, J.-A; Kim, M.-K.; Paek, H.-J.; Kim, Y.-R.; Kim, M.-K.; Lee, J.-K.; Jeong, J.; Choi, S.-J. Tissue Distribution and Excretion Kinetics of Orally Administered Silica Nanoparticles in Rats. *Int. J. Nanomedicine* **2014**, *9*, 251−60.
(124) Haute, D. V.; Berlin, J. M. Challenges in Realizing Selectivity for Nanoparticle Biodistribution and Clearance: Lessons from Gold Nanoparticles. *Ther. Delivery* **2017**, *8*, 763−774.
(125) Tsoi, K. M.; MacParland, S. A.; Ma, X. Z.; Spetzler, V. N.; Echeverri, J.; Ouyang, B.; Fadel, S. M.; Sykes, E. A.; Goldaracena, N.; Kaths, J. M.; Conneely, J. B.; Alman, B. A.; Selzner, M.; Ostrowski, M. A.; Adeyi, O. A.; Zilman, A.; McGilvray, I. D.; Chan, W. C. Mechanism of Hard-Nanomaterial Clearance by the Liver. *Nat. Mater.* **2016**, *15*, 1212−1221.
(126) Poon, W.; Zhang, Y. N.; Ouyang, B.; Kingston, B. R.; Wu, J. L. Y.; Wilhelm, S.; Chan, W. C. W. Elimination Pathways of Nanoparticles. *ACS Nano* **2019**, *13*, 5785−5798.
(127) Zhang, Y. N.; Poon, W.; Tavares, A. J.; McGilvray, I. D.; Chan, W. C. Nanoparticle−Liver Interactions: Cellular Uptake and Hepatobiliary Elimination. *J. Controlled Release* **2016**, *240*, 332−348.
(128) Tavares, A. J.; Poon, W.; Zhang, Y.-N.; Dai, Q.; Besla, R.; Ding, D.; Ouyang, B.; Li, A.; Chen, J.; Zheng, G.; et al. Effect of Removing Kupffer Cells on Nanoparticle Tumor Delivery. *Proc. Natl. Acad. Sci. U. S. A.* **2017**, *114*, E10871−E10880.
(129) Yin, R.; Zhang, X.; Ge, J.; Wen, L.; Chen, L.; Zeng, J.; Li, Z.; Gao, M. Recent Advances in Renal Clearable Inorganic Nanoparticles for Cancer Diagnosis. *Part. Part. Syst. Charact* **2021**, *38*, 2000270.
(130) Liang, X.; Wang, H.; Zhu, Y.; Zhang, R.; Cogger, V. C.; Liu, X.; Xu, Z. P.; Grice, J. E.; Roberts, M. S. Short-and Long-Term Tracking of Anionic Ultrasmall Nanoparticles in Kidney. *ACS Nano* **2016**, *10*, 387−395.
(131) Yu, M.; Zhou, C.; Liu, L.; Zhang, S.; Sun, S.; Hankins, J. D.; Sun, X.; Zheng, J. Interactions of Renal-Clearable Gold Nanoparticles with Tumor Microenvironments: Vasculature and Acidity Effects. *Angew. Chem., Int. Ed. Engl.* **2017**, *129*, 4378−4383.
(132) Balogh, L.; Nigavekar, S. S.; Nair, B. M.; Lesniak, W.; Zhang, C.; Sung, L. Y.; Kariapper, M. S.; El-Jawahri, A.; Llanes, M.; Bolton, B.; Mamou, F.; Tan, W.; Hutson, A.; Minc, L.; Khan, M. K. Significant Effect of Size on the in Vivo Biodistribution of Gold Composite Nanodevices in Mouse Tumor Models. *Nanomedicine* **2007**, *3*, 281−96.
(133) Kanazaki, K.; Sano, K.; Makino, A.; Shimizu, Y.; Yamauchi, F.; Ogawa, S.; Ding, N.; Yano, T.; Temma, T.; Ono, M.; Saji, H. Development of Anti-Her2 Fragment Antibody Conjugated to Iron Oxide Nanoparticles for in Vivo Her2-Targeted Photoacoustic Tumor Imaging. *Nanomedicine* **2015**, *11*, 2051−60.
(134) Mahmoudi, M.; Landry, M. P.; Moore, A.; Coreas, R. The Protein Corona from Nanomedicine to Environmental Science. *Nature Reviews Materials* **2023**, *8*, 422−438.
(135) Yuan, L.; Chen, Q.; Riviere, J. E.; Lin, Z. Pharmacokinetics and Tumor Delivery of Nanoparticles. *Journal of Drug Delivery Science and Technology* **2023**, *83*, 104404.
(136) Saptarshi, S. R.; Duschl, A.; Lopata, A. L. Interaction of Nanoparticles with Proteins: Relation to Bio-Reactivity of the Nanoparticle. *J. Nanobiotechnology* **2013**, *11*, 26.
(137) Brown, R. P.; Delp, M. D.; Lindstedt, S. L.; Rhomberg, L. R.; Beliles, R. P. Physiological Parameter Values for Physiologically Based Pharmacokinetic Models. *Toxicol. Ind. Health.* **1997**, *13*, 407−484.
(138) Strojan, K.; Leonardi, A.; Bregar, V. B.; Križaj, I.; Svete, J.; Pavlin, M. Dispersion of Nanoparticles in Different Media Importantly Determines the Composition of Their Protein Corona. *PloS one* **2017**, *12*, No. e0169552.
(139) Ross, A. M.; Kennedy, T.; McNulty, D.; Leahy, C. I.; Walsh, D. R.; Murray, P.; Grabrucker, A. M.; Mulvihill, J. J. E. Comparing Nanoparticles for Drug Delivery: The Effect of Physiological Dispersion Media on Nanoparticle Properties. *Mater. Sci. Eng. C Mater. Biol. Appl.* **2020**, *113*, 110985.
(140) Rosner, B. Percentage Points for a Generalized Esd Many-Outlier Procedure. *Technometrics* **1983**, *25*, 165−172.
(141) Lin, Z.; Chou, W. C.; Cheng, Y. H.; He, C.; Monteiro-Riviere, N. A.; Riviere, J. E. Predicting Nanoparticle Delivery to Tumors Using Machine Learning and Artificial Intelligence Approaches. *Int. J. Nanomedicine* **2022**, *17*, 1365−1379.
(142) Chou, W. C.; Chen, Q.; Yuan, L.; Cheng, Y. H.; He, C.; Monteiro-Riviere, N. A.; Riviere, J. E.; Lin, Z. An Artificial Intelligence-Assisted Physiologically-Based Pharmacokinetic Model to Predict Nanoparticle Delivery to Tumors in Mice. *J. Controlled Release* **2023**, *361*, 53−63.
(143) Sindhwani, S.; Chan, W. C. W. Nanotechnology for Modern Medicine: Next Step Towards Clinical Translation. *J. Intern Med.* **2021**, *290*, 486−498.
(144) Chou, W. C.; Cheng, Y. H.; Riviere, J. E.; Monteiro-Riviere, N. A.; Kreyling, W. G.; Lin, Z. Development of a Multi-Route Physiologically Based Pharmacokinetic (Pbpk) Model for Nanomaterials: A Comparison between a Traditional Versus a New Route-Specific Approach Using Gold Nanoparticles in Rats. *Part Fibre Toxicol* **2022**, *19*, 47.

https://doi.org/10.1021/acsnano.3c04037
ACS Nano 2023, 17, 19810−19831

(145) Douglas, C. E.; Michael, F. A. On Distribution-Free Multiple Comparisons in the One-Way Analysis of Variance. *Commun. Stat.* **1991**, *20*, 127−139.
(146) Dwass, M. *Some K-Sample Rank Order Tests In Contributions to Probability and Statistics;* Stanford University Press: Stanford, CA, 1960; pp 198−202.
(147) Steel, R. G. A Rank Sum Test for Comparing All Pairs of Treatments. *Technometrics* **1960**, *2*, 197−207.
(148) R Core Team, R. *A Language and Environment for Statistical Computing;* R Foundation for Statistical Computing: Vienna, Austria, 2022.

https://doi.org/10.1021/acsnano.3c04037
ACS Nano 2023, 17, 19810−19831